

Complete positive operator-valued measure description of multichannel quantum electro-optic sampling with monochromatic field modes

Emanuel Hubenschmid^{⊗,*}, Thiago L. M. Guedes^{⊗,†} and Guido Burkard^{⊗,‡}
Department of Physics, University of Konstanz, 78457 Konstanz, Germany

 (Received 1 July 2022; accepted 3 October 2022; published 19 October 2022)

We propose a multichannel version of quantum electro-optic sampling involving monochromatic field modes. It allows for multiple simultaneous measurements of arbitrarily many \hat{X} and \hat{Y} field quadratures for a single quantum-state copy, while independently tuning the interaction strengths at each channel. In contrast to standard electro-optic sampling, the sampled midinfrared (MIR) mode undergoes a nonlinear interaction with multiple near-infrared pump beams. We present a complete positive operator-valued measure description for quantum states in the MIR mode. The probability distribution of the electro-optic signal outcomes is shown to be related to an s -parametrized phase-space quasiprobability distribution of the indirectly measured MIR state, with the parameter s depending solely on the quantities characterizing the nonlinear interaction. Furthermore, we show that the quasiprobability distributions for the sampled and postmeasurement states are related to each other through a renormalization and a change in the parametrization. This result is then used to demonstrate that two consecutive measurements of both \hat{X} and \hat{Y} quadratures can outperform eight-port homodyne detection.

DOI: [10.1103/PhysRevA.106.043713](https://doi.org/10.1103/PhysRevA.106.043713)

I. INTRODUCTION

Understanding simultaneous measurements of incompatible observables is key to differentiate quantum mechanics from classical physics. That a quantum theory must inevitably be of a statistical nature was already recognized in the early days of quantum mechanics and led to Heisenberg's uncertainty principle [1–3]. As a consequence thereof, it is not possible to prepare an ensemble with dispersion-free conjugate variables such as position and momentum. The quantum states of a system in conventional quantum mechanics thus cannot be represented as points in phase space, unlike in classical mechanics, but require instead a description that captures this fundamental limitation. Here the question could arise whether the quantum-mechanical expectation value can be calculated as an ensemble average over a phase-space function, as in classical statistical mechanics. One of the most widely known attempts to formulate quantum mechanics in terms of phase-space distributions was made by Wigner [4]. Although the quantum-state phase-space function proposed by Wigner gives the correct probabilities for the position and momentum as marginal distributions, it can take negative values and does not allow for an interpretation as a probability distribution; for this reason, it is often referred to as a quasiprobability distribution. However, the Wigner function is not the only phase-space distribution which, together with a properly chosen phase-space function representing the observable, gives the same expectation value as von Neumann's trace formula (see [5], p. 207). In fact, there is a large

family of distributions fulfilling this condition, as shown by Cohen [6].

Wigner later proved that there is no positive phase-space distribution, which is linear as a function of the density operator, with the correct quantum-mechanical marginal distributions [7]. Thus, if we want to directly sample a quasiprobability distribution and obtain the marginal distribution thereof, there will be some additional uncertainty. Arthurs and Kelly [8,9] obtained the same result by applying von Neumann's indirect measurements (see [5], Chap. VI.3) to a (specific) simultaneous measurement. Werner [10] formalized this notion by distinguishing between preparation and measurement uncertainty and derived uncertainty relations for those.

Simultaneous measurements were realized for various physical systems, such as a transmon qubit in a microwave cavity [11,12], an optical qubit [13–15], or a single mode of light [16,17]. In the case of the quantized electromagnetic field, the vector potential assumes the role of the generalized coordinate. For monochromatic field modes, the vector potential is proportional to the $\hat{X} = \frac{1}{2}(\hat{a} + \hat{a}^\dagger)$ quadrature, in which \hat{a} is the bosonic annihilation operator of the field mode, and the corresponding canonical conjugate is the electric-field-related $\hat{Y} = \frac{i}{2}(\hat{a}^\dagger - \hat{a})$ quadrature (see [18], p. 94, and [19]). This allows one to describe a single-mode quantum state of the electromagnetic-field mode using quasiprobability distributions. There are several optical methods to sample specific quasiprobability distributions, such as the many variants of homodyne detection to measure the quadratures either separately [20–29] or simultaneously [16,17,30–32]. One such possibility is to use eight-port homodyne detection, in which the sampled mode is split into two modes using a beam splitter and then the two quadratures can be measured simultaneously using a four-port homodyne detection scheme

*emanuel.hubenschmid@uni-konstanz.de

†thiago.lucena@uni-konstanz.de

‡guido.burkard@uni-konstanz.de

[17]. Another possibility to measure the field quadratures is provided by quantum electro-optic sampling (EOS) [33–43]. Electro-optic sampling is an indirect measurement of low-frequency modes, usually in the midinfrared (MIR), mediated by higher-frequency modes, usually in the near infrared (NIR). For this to happen, modes in the two frequency ranges are correlated by an interaction in a nonlinear crystal [44,45]. Subsequently, all the high-frequency modes are sampled by a single detection stage, which limits this configuration to the measurement of a single quadrature at a time. However, the simultaneous measurement of two noncommuting quadratures is of great interest to many applications in quantum information technologies, such as quantum metrology [46–49], continuous-variable quantum teleportation [50,51], and continuous-variable quantum key distribution [52,53]. A particular example consists in the case of a double quantum-dot charge qubit where it was shown that cross correlations between simultaneously measured charge-detector signals allow for the improvement of the signal-to-noise ratio [54].

In this paper we show that a multichannel version of (continuous-wave-driven) electro-optic sampling can be utilized to sample quasiprobability distributions of a monochromatic MIR quantum state and thus overcome the limitation of EOS to measurements of a single quadrature. We explicitly demonstrate this by calculating the count-probability distribution (12). Differently from the standard approach to electro-optic sampling, multiple monochromatic NIR modes assigned to different channels are sampled by different detection stages. This allows one to simultaneously measure multiple quadratures of a single MIR state and to tune the interaction strength between the MIR and each NIR mode individually. Thus, the model presented in this paper is applicable to arbitrary many measurements of \hat{X} and/or \hat{Y} quadratures. Furthermore, we derive the postmeasurement quasiprobability distributions for arbitrary combinations of \hat{X} - and/or \hat{Y} -quadrature measurements [Eq. (24)] and use this result to show that additional measurements on the postmeasurement state can outperform eight-port homodyne detection.

In Sec. II the proposed measurement scheme and the respective theoretical model are presented. In Sec. III the count-probability distribution is derived and some special cases are discussed. In Sec. IV we show how the quasiprobability distribution for the postmeasurement state relates to the initial states one. In Sec. V the different measurement schemes based on electro-optic sampling are compared and it is shown that two consecutive measurements of the same state can outperform eight-port homodyne detection.

II. MODEL

As is the case for any quantum-mechanical indirect measurement, electro-optic sampling makes use of an ancillary system (in the present case, the high-frequency NIR modes of the electric field), which becomes correlated with the low-frequency mode of the field (here the MIR) through interactions in a nonlinear crystal [33–44]. We consider the specific case of an optical parametric oscillator consisting of a zinc-blende-type nonlinear crystal in a cavity, labeled as (i) in Fig. 1(a). The details about the geometrical arrangement

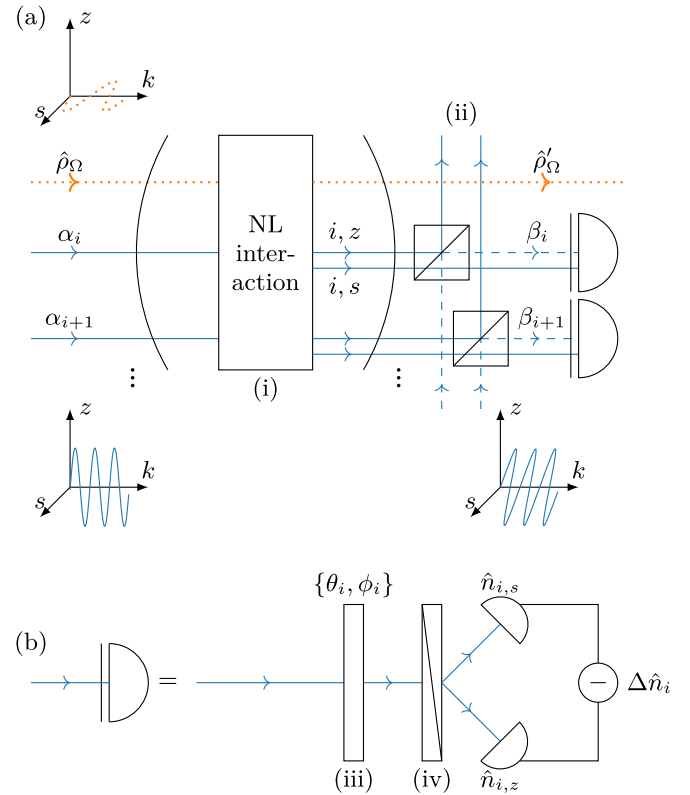


FIG. 1. Schematic representation of the proposed measurement setup. The first step in (a) is a nonlinear interaction between the NIR pump beams with amplitudes α_i and the MIR mode $\hat{\rho}_\Omega$ in the optical parametric oscillator (i). Then the z -polarized components of the NIR cavity frequencies are filtered out and replaced by z -polarized probe beams β_i using the polarizing beam splitter (ii). Subsequently, the quadratures of the NIR modes are measured using the ellipsometry scheme depicted in (b). The ellipsometer consists of the ϕ_i waveplate (iii) rotated by θ_i , a polarizing beam splitter (iv) to separate the s - and z -polarized photons of the NIR frequencies, and two photon detectors to count the photon number of each polarization. The difference between the s - and z -polarized photon numbers $\Delta \hat{n}_i = \hat{n}_{i,s} - \hat{n}_{i,z}$ constitutes the signal.

of the nonlinear crystal are given in [35]. In the crystal, the coherent z -polarized pump beams in the NIR cavity modes $i \in I = \{1, 2, \dots\}$, with amplitudes α_i , drive the entanglement between the s -polarized NIR modes, corresponding to the bosonic operator $\hat{a}_{i,s}$, and the s -polarized MIR mode, related to $\hat{a}_{\Omega,s}$. This nonlinear interaction is described by the multi-mode squeezing operator (see [18], pp. 276–281)

$$\hat{U}_{\text{NL}} = \exp \left(\zeta^* \hat{a}_{\Omega,s} \sum_{i \in I} \tilde{\alpha}_i \hat{a}_{i,s} - \text{H.c.} \right), \quad (1)$$

where ζ is the dressed squeezing parameter and $\tilde{\alpha}_i = \alpha_i / (\sum_{i \in I} |\alpha_i|^2)^{1/2}$ the normalized pump amplitude. The time-evolution operator (1) is therefore an effective two-mode squeezing operator between $\hat{a}_{\Omega,s}$ and $\sum_{i \in I} \tilde{\alpha}_i \hat{a}_{i,s}$. This effective two-mode description is achieved by absorbing the normalization constant of the α_i into the undressed squeezing parameter ζ_0 .

After the nonlinear interaction, the z -polarized NIR pump beams are filtered out by the polarizing beam splitters (ii) and coherent NIR probes of amplitudes β_i are introduced as replacements. The z -polarized NIR modes are therefore displaced by $\hat{D}_{i,z}(\beta_i) = \exp(\beta_i \hat{a}_{i,z}^\dagger - \text{H.c.})$. This allows for an additional, tunable set of parameter. If a setup without this filtering is considered, the pump amplitudes α_i can be set equal to the probe amplitudes β_i .

The quadratures of the (s -polarized) NIR field modes are then measured using ellipsometers [33,35,55]. The first step of the ellipsometry scheme, (iii) in Fig. 1(b), is the change in the ellipticities of the joint-polarization NIR modes due to a ϕ_i waveplate rotated by an angle θ_i relative to the z axis, $\hat{U}_{i,\text{WP}} = \exp(i\phi_i \hat{a}_{i,\theta}^\dagger \hat{a}_{i,\theta})$. Here $\hat{a}_{i,\theta} = \cos(\theta_i) \hat{a}_{i,s} + \sin(\theta_i) \hat{a}_{i,z}$ are the annihilation operators of the modes the waveplate acts on. The total time-evolution operator is thus

$$\hat{U} = \hat{U}_{\text{WP}} \hat{D}_z(\vec{\beta}) \hat{U}_{\text{NL}}. \quad (2)$$

To allow for a compact notation we have introduced the total waveplate operator $\hat{U}_{\text{WP}} = \bigotimes_{i \in I} \hat{U}_{i,\text{WP}}$ and the total displacement operator $\hat{D}_z(\vec{\beta}) = \bigotimes_{i \in I} \hat{D}_{i,z}(\beta_i)$.

In a second step, denoted by (iv) in Fig. 1(b), the photons at each NIR cavity frequency i are split spatially into s -polarized and z -polarized contributions with the aid of a polarizing beam splitter. Finally, the photons of each polarization are counted using photon detectors and the number of z -polarized counts is subtracted from the s -polarized ones. The corresponding observables are thus the difference between the respective photon-number operators at each cavity frequency i ,

$$\Delta \hat{n}_i = \hat{n}_{i,s} - \hat{n}_{i,z} = \sum_{\Delta n_i = -\infty}^{\infty} \Delta n_i \hat{P}_{\Delta n_i}. \quad (3)$$

In order to obtain a description in terms of positive operator-valued measures (POVMs), the observables are decomposed into the projectors on the subspace of states with photon-number difference Δn_i between the s -polarized and the z -polarized NIR counts at frequency i ,

$$\hat{P}_{\Delta n_i} = \sum_{n_i = \tilde{n}_i}^{\infty} |n_i + \Delta n_i\rangle_{i,s} \langle n_i + \Delta n_i| \otimes |n_i\rangle_{i,z} \langle n_i|, \quad (4)$$

where the summation starts at $\tilde{n}_i = \max\{0, -\Delta n_i\}$ to avoid negative photon-number occupations. These are the necessary components to calculate the count probability of the photon-number differences $\{\Delta n_i\} = \{\Delta n_i \mid i \in I\}$.

III. COUNT-PROBABILITY DISTRIBUTION

The probability distribution

$$p(\{\Delta n_i\}) = \text{tr}(\hat{P}_{\{\Delta n_i\}} \hat{\rho}_\Omega \otimes |0\rangle_\omega \langle 0| \hat{U}^\dagger) \quad (5)$$

to measure the set of photon-number differences $\{\Delta n_i\}$ is the expectation value of the projector $\hat{P}_{\{\Delta n_i\}} = \bigotimes_{i \in I} \hat{P}_{\Delta n_i}$ with respect to the time-evolved state $\hat{U} \hat{\rho}_\Omega \otimes |0\rangle_\omega \langle 0| \hat{U}^\dagger$. The density operator $\hat{\rho}_\Omega$ corresponds to the initial state of the s -polarized MIR mode of the electromagnetic field and $|0\rangle_\omega = \bigotimes_{i \in I} |0\rangle_{i,s} \otimes |0\rangle_{i,z}$ is the vacuum of the NIR modes. The density operator is expressed in the coherent-state basis $|z\rangle_\Omega = \hat{D}_\Omega(z)|0\rangle_\Omega$ of the MIR Hilbert space [which is generated

by displacing the vacuum with $\hat{D}_\Omega(z) = \exp(z \hat{a}_{\Omega,s}^\dagger + \text{H.c.})$] using the Glauber-Sudarshan quasiprobability distribution $\rho(z; s = 1)$ of the sampled MIR state [56,57],

$$\hat{\rho}_\Omega = \int \rho(z; 1) |z\rangle_\Omega \langle z| d^2z. \quad (6)$$

The same is done with the projector $\hat{P}_{\Delta n_i}$, defined in Eq. (4). The probability distribution in Eq. (5) is therefore expressed completely in the coherent-state basis, resulting in convolutions of the Glauber-Sudarshan distributions with the matrix elements of the evolution operator in the coherent-state basis (cf. Appendix A). Furthermore, it can be shown that this is equivalent to a convolution of the MIR Glauber-Sudarshan distribution and the Skellam distribution, which is the probability distribution of the difference Δn_i between two Poissonian counting events. This is the statistics expected from the ellipsometry scheme in Fig. 1(b), since the signal is the difference between two (predominantly) Poissonian photon-number counting events (because the modes at the photon detectors are dominated by the coherent-probe amplitudes β_i and the photon-number distribution for coherent states is Poissonian).

We want the electro-optic signal to be balanced, which means that the signal is on average zero as long as the MIR mode is in a state for which all quadrature expectation values vanish (e.g., the vacuum). This way, noise affecting both polarizations of the NIR frequencies cancel out in the ellipsometry scheme. We achieve this by choosing the rotation angle of the ϕ_i waveplate as

$$\theta_i = (-1)^{k_1} \frac{1}{2} \arccos \left\{ (-1)^{k_2} \sqrt{\frac{1}{2} \left[1 - \cot^2 \left(\frac{\phi_i}{2} \right) \right]} \right\}, \quad (7)$$

which has solutions for $\frac{\pi}{2} \leq \phi_i \leq \frac{3}{2}\pi$ and $k_1, k_2 \in \mathbb{Z}$. With this choice, the complex phase determining the interference at the i th ellipsometry is given by

$$\phi_i = \left\{ (k_1 + k_2 + 1)\pi + (-1)^{k_2} \arcsin \left[\sqrt{2} \cos \left(\frac{\phi_i}{2} \right) \right] + \arg(\zeta) - \arg(\tilde{\alpha}_i) - \arg(\beta_i) \right\} \text{mod} 2\pi \quad (8)$$

as can be seen from Eqs. (A12), (A14), and (A16). Choosing the signal to be balanced additionally allows us to approximate the Skellam distribution by a Gaussian, as long as the probe amplitudes $|\beta_i|$ are large compared to the average photon number of the MIR state (see Appendix B for details). This enables an analytical calculation of the convolution.

Before the count-probability distribution is presented, we have to introduce a special family of quasiprobability distributions. The standard s -parametrized quasiprobability distribution $\rho(z; s) = 1/\pi^2 \int \exp(z\gamma^* - z^*\gamma) \chi(\gamma; s) d^2\gamma$ with the s -parametrized characteristic function $\chi(\gamma; s) = \exp(s|\gamma|^2) \hat{D}(\gamma)$ (see [58,59] and [18], p. 128) is not sufficient to capture all the different cases our model describes. This is why we have to introduce the (s_X, s_Y) -parametrized quasiprobability distribution

$$\rho(z; s_X, s_Y) = \frac{1}{\pi^2} \int e^{z\gamma^* - z^*\gamma} \chi(\gamma; s_X, s_Y) d^2\gamma, \quad (9)$$

defined in terms of the (s_X, s_Y) -parametrized characteristic function

$$\chi(\gamma; s_X, s_Y) = \chi(\gamma; 0) e^{(s_Y/2)\text{Re}^2(\gamma) + (s_X/2)\text{Im}^2(\gamma)}. \quad (10)$$

This is a special case of the generalized quasiprobability distribution using a Cohen function $f(\gamma) = \exp[s_X \text{Re}^2(\gamma)/2 + s_Y \text{Im}^2(\gamma)/2]$ [6].

For $s_X, s_Y < 1$, the two-parameter quasiprobability distribution can be expressed as a Weierstrass transform of the Glauber-Sudarshan distribution

$$\begin{aligned} \rho(z; s_X, s_Y) &= \frac{1}{\pi} \frac{2}{\sqrt{(1-s_X)(1-s_Y)}} \int \rho(y; 1) \\ &\times \exp\left(-\frac{2}{1-s_X} \text{Re}^2(y-z) - \frac{2}{1-s_Y} \text{Im}^2(y-z)\right) d^2y. \end{aligned} \quad (11)$$

We can cast the count-probability distribution after application of the Gaussian approximation to the Skellam distribution [cf. Eq. (A19)] into the form of the (s_X, s_Y) -parametrized quasiprobability distribution in Eq. (11) if we partition the set of all NIR frequencies into two disjoint sets I_X and I_Y , with $I = I_X \cup I_Y$ and $I_X \cap I_Y = \emptyset$. If the angles of the waveplates are then chosen such that $e^{i\varphi_{i_X}} = 1$ for all $i_X \in I_X$ and $e^{i\varphi_{i_Y}} = i$ for all $i_Y \in I_Y$, then the count-probability distribution

$$p(\{\Delta n_i\}) \approx N(\{\Delta n_i\}) \rho(z(\{\Delta n_i\}); \tilde{s}_X, \tilde{s}_Y) \quad (12)$$

is given in terms of the two-parameter quasiprobability distribution $\rho(z(\{\Delta n_i\}); \tilde{s}_X, \tilde{s}_Y)$, as well as a renormalization envelope

$$\begin{aligned} N(\{\Delta n_i\}) &= \pi \frac{\sqrt{(1-\tilde{s}_X)(1-\tilde{s}_Y)}}{2\sqrt{1+A_X}\sqrt{1+A_Y}} \prod_{i \in I} \frac{e^{-\Delta n_i^2/2|\beta_i|^2}}{\sqrt{2\pi|\beta_i|^2}} \\ &\times \exp\left\{-\frac{2\text{Re}^2[z(\{\Delta n_i\})]}{1+\tilde{s}_X} - \frac{2\text{Im}^2[z(\{\Delta n_i\})]}{1+\tilde{s}_Y}\right\}, \end{aligned} \quad (13)$$

with $\mu = \cosh(|\zeta|)$, $\nu = \exp[i \arg(\zeta)] \sinh(|\zeta|)$, and the rescaled, combined pump strength $A_Q = 2|\nu|^2 \sum_{i_Q} |\tilde{\alpha}_{i_Q}|^2$, where Q is from now on used as a placeholder for both X and Y . As will become clear later, the set I_X (I_Y) corresponds to \hat{X} - (\hat{Y} -)quadrature measurements.

The parameters

$$\tilde{s}_Q = 1 - \frac{2}{1 + (1 + A_Q)^{-1}}, \quad (14)$$

with $Q = X, Y$, solely depend on quantities characterizing the interaction between the NIR and MIR modes. If the sum of the probe amplitudes for the \hat{X} measurements equals that for the \hat{Y} measurements $A_X = A_Y = |\nu|^2$, the parameter $\tilde{s} = \tilde{s}_X = \tilde{s}_Y$ is a function of the squeezing parameter $|\zeta|$, as depicted in Fig. 2. The argument of the quasiprobability distribution in Eq. (12) is related to the photon-number differences $\{\Delta n_i\}$

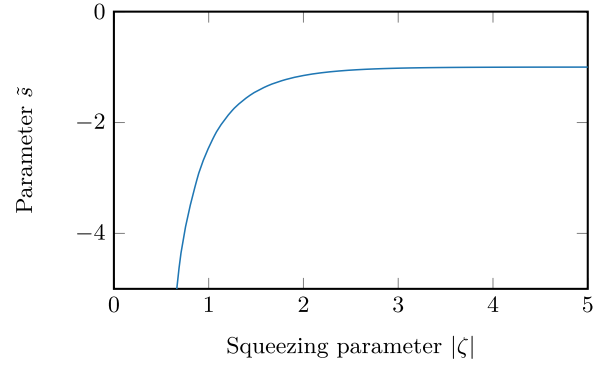


FIG. 2. Parameter \tilde{s} for a measurement with equal probe amplitudes $A_X = A_Y$ as a function of the squeezing strength $|\zeta|$.

via

$$\begin{aligned} z(\{\Delta n_i\}) &= -|\nu| \left(\frac{1 + \tilde{s}_X}{2} \sum_{i_X \in I_X} \frac{|\tilde{\alpha}_{i_X}|}{|\beta_{i_X}|} \Delta n_{i_X} \right. \\ &\left. + i \frac{1 + \tilde{s}_Y}{2} \sum_{i_Y \in I_Y} \frac{|\tilde{\alpha}_{i_Y}|}{|\beta_{i_Y}|} \Delta n_{i_Y} \right). \end{aligned} \quad (15)$$

The distribution in Eq. (12) is the main result of this work and corresponds to the most general form of the count-probability distribution for the setup in Fig. 1.

Let us highlight the special case with one \hat{X} measurement and one \hat{Y} measurement, i.e., $|I_X| = |I_Y| = 1$, and equal combined pump amplitudes ($A_X = A_Y$) for the \hat{X} and \hat{Y} measurements. We will call this measurement a symmetric $\bar{X}\bar{Y}$ measurement from now on. For this configuration, the renormalization envelope $N(\{\Delta n_i\}) = (2|\nu|^2 |\beta_1| |\beta_2|)^{-1}$ is constant. An example of the corresponding count-probability distribution, with a three-photon Fock state as an MIR input, can be seen in Fig. 3.

For weak squeezing $\zeta = 0.1$ the distribution is dominated by the vacuum in the NIR modes, while for stronger squeezing $\zeta = 1$ the contribution of the MIR state becomes much clearer. This setup is similar to eight-port homodyne detection as considered by Freyberger *et al.* [17]. The approximation used in [17] is a special case of the Gaussian approximation to the Skellam distribution. While the two approximations coincide for the symmetric $\bar{X}\bar{Y}$ measurement, the former breaks down for a simultaneous measurement of more than two quadratures. The approximation of the Skellam distribution, on the other hand, is valid for arbitrarily many measurements. On top of that, it gives physical intuition of the processes at the ellipsometry stage, as explained in Sec. III. In eight-port homodyne detection, the probability distribution is related to the Husimi function $\rho(z; s = -1)$ [60], as long as perfect detectors are considered. This corresponds to the limit of infinite squeezing: $\lim_{|\zeta| \rightarrow \infty} \tilde{s} = -1$. If the detectors have a quantum efficiency $\eta < 1$ or the first beam splitter in the eight-port homodyne setup is replaced by a down-conversion process, the parameter \tilde{s} of the sampled quasiprobability distribution can also be smaller than -1 [27,30,31]. In contrast to homodyne detection, electro-optic sampling is an indirect measurement. This allows us not only to tune the strength of the measurement (so that backaction on the sampled MIR state

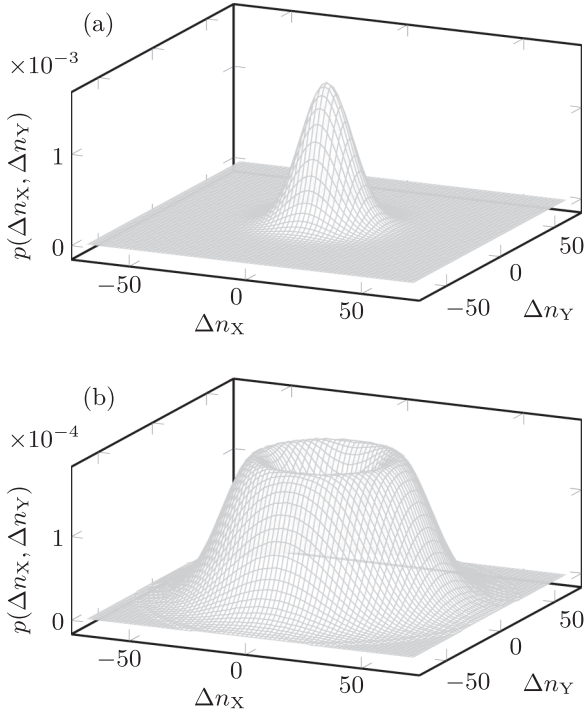


FIG. 3. Example of the count-probability distribution $p(\Delta n_X, \Delta n_Y)$ corresponding to a symmetric $\bar{X}\bar{Y}$ measurement with equal pump strengths $|\tilde{\alpha}_X| = |\tilde{\alpha}_Y| = 1/\sqrt{2}$ and probes $\beta_X = \beta_Y = 10$ of a three-photon MIR Fock state $n_\Omega = 3$. In (a) the squeezing strength is assumed to be $\zeta = 0.1$ and in (b) it is assumed to be $\zeta = 1$. Although the photon-number differences are discrete, the distribution is broad enough to justify the use of a continuous surface plot.

can be kept at a desired level [61]), but also to investigate the postmeasurement state in the MIR, since the indirect sampling is by nature nondestructive. The two measurement schemes are compared further in Sec. V.

A. Ensemble limit

The probability distribution (12) can be used to calculate the expected photon-number differences $\langle \Delta n_i \rangle$, as well as the corresponding variances $\sigma_{\Delta n_i}^2$. Let us consider the symmetric $\bar{X}\bar{Y}$ measurement from the preceding section. The expectation value for, e.g., the first photon-number difference is then

$$\langle \Delta n_X \rangle = \sum_{\Delta n_X, \Delta n_Y = -\infty}^{\infty} \Delta n_X p(\Delta n_X, \Delta n_Y). \quad (16)$$

For a strong probe, such that $|\beta_i||v|$ is large, the sum can be approximated by an integral: $\langle \Delta n_X \rangle \approx \sqrt{2}|v||\beta_X| \int \text{Re}(z)\rho(z; s)d^2z$. This is a phase-space average and can thus be related to the (ensemble) expectation values of the MIR \hat{X} quadrature, so for $\hat{X}_\Omega = \frac{1}{2}(\hat{a}_\Omega + \hat{a}_\Omega^\dagger)$ and $\hat{Y}_\Omega = \frac{i}{2}(\hat{a}_\Omega^\dagger - \hat{a}_\Omega)$ one has

$$\langle \Delta n_Q \rangle \approx \sqrt{2}|v||\beta_Q|\langle \hat{Q}_\Omega \rangle, \quad (17)$$

with $Q = X, Y$. Similarly, the (root-mean-square) variances of the photon-number differences can be related to the

variances of the quadratures, $\sigma_X^2 = \langle \hat{X}_\Omega^2 \rangle - \langle \hat{X}_\Omega \rangle^2$ and $\sigma_Y^2 = \langle \hat{Y}_\Omega^2 \rangle - \langle \hat{Y}_\Omega \rangle^2$, according to

$$\sigma_{\Delta n_Q}^2 \approx 2|v|^2|\beta_Q|^2(\sigma_Q^2 - \frac{\bar{s}}{4}). \quad (18)$$

While the probe amplitudes β_Q rescale the quasiprobability distribution, the Weierstrass transform smoothes it, resulting in additional noise. The variance in Eq. (18) consists of two contributions scaled by the same factor $\sqrt{2}|v||\beta_Q|$ as the quadrature expectation value in Eq. (17): The first contribution comes from the unperturbed variance of the MIR-state quadratures σ_Q^2 , so the product $\sigma_X^2\sigma_Y^2 \geq \frac{1}{16}$ is limited by Robertson's uncertainty relation [62]; the second contribution is proportional to the parameter \bar{s} and is independent of the sampled state. Thus the first contribution can be attributed to the preparation uncertainty, while the second term relates to the measurement uncertainty. As shown by Werner [3,10], these uncertainty relations coincide. In this case, they are both bounded by $\frac{1}{16}$, i.e., $\bar{s}^2/16 \geq \frac{1}{16}$ and $\sigma_X^2\sigma_Y^2 \geq \frac{1}{16}$. This bound is optimal for the simultaneous measurement of a single observable, which is a function of generalized position and momentum [3]. The relation $(\sigma_X^2 - \bar{s}/4)(\sigma_Y^2 - \bar{s}/4) \geq \frac{1}{4}$ also agrees with the result from Arthurs and Goodman [9] about balanced homodyne detection.

B. Marginal distributions

The marginal distributions of the Wigner function $\rho(z; s = 0)$ give the correct quantum mechanical probabilities for the generalized coordinate and conjugate momentum [4]. Thus, we express the (s_X, s_Y) -parametrized quasiprobability distribution for $s_X, s_Y < 0$ as

$$\rho(z; s_X, s_Y) = \frac{1}{\pi} \frac{2}{\sqrt{s_X s_Y}} \int \rho(y; 0) \times e^{2\text{Re}^2(y-z)/s_X + 2\text{Im}^2(y-z)/s_Y} d^2y. \quad (19)$$

If only \hat{X} (\hat{Y}) measurements are considered, the opposite-quadrature parameter \tilde{s}_Y (\tilde{s}_X) goes to $-\infty$ as the pump amplitude for the \hat{Y} (\hat{X}) measurement vanishes: $|\tilde{\alpha}_{iY}| \rightarrow 0$ ($|\tilde{\alpha}_{iX}| \rightarrow 0$). Thus, the probability distribution of sole \hat{X} measurements is related to the marginal distribution of the Wigner function $\langle x|\hat{\rho}_\Omega|x\rangle_\Omega$,

$$p(\{\Delta n_i\}) \approx N_X(\{\Delta n_i\}) \int_\Omega \langle x|\hat{\rho}_\Omega|x\rangle_\Omega \times e^{(2/\tilde{s}_X)\{x - \text{Re}[z(\{\Delta n_i\})]\}^2} dx, \quad (20)$$

with the renormalization envelope

$$N_X(\{\Delta n_i\}) = \frac{\sqrt{1 - \tilde{s}_X}/\sqrt{-\tilde{s}_X}}{\mu^2 \sqrt{1 - \mu^4/|v|^4}} \prod_{i \in I} \frac{e^{-\Delta n_i^2/2|\beta_i|^2}}{\sqrt{2\pi|\beta_i|^2}} \times \exp \left\{ \left[1 + 2 \frac{v^2 + \mu^2}{1 - \tilde{s}_X} \right] \frac{2\text{Re}^2[z(\{\Delta n_i\})]}{1 - \tilde{s}_X} \right\}. \quad (21)$$

Analogously, the probability distribution for only \hat{Y} measurements is related to the quantum-mechanical distribution of the \hat{Y} quadrature, $\langle y|\hat{\rho}_\Omega|y\rangle_\Omega$, with the roles of X and Y interchanged and $\text{Re}[z(\{\Delta n_i\})]$ replaced by $\text{Im}[z(\{\Delta n_i\})]$.

The count-probability distribution is not directly given by the quantum-mechanical distribution, but by its Weierstrass transform, resulting in a distribution smoothing that manifests itself as additional noise.

IV. POSTMEASUREMENT QUASIPROBABILITY DISTRIBUTION

The state in the MIR mode after the measurement is

$$\hat{\rho}'_{\Omega} = \frac{1}{p(\{\Delta n_i\})} \sum_{\{n_i\}} \hat{M}_{\{n_i, \Delta n_i\}} \hat{\rho}_{\Omega} \hat{M}_{\{n_i, \Delta n_i\}}^{\dagger}, \quad (22)$$

with the measurement operator

$$\hat{M}_{\{n_i, \Delta n_i\}} = \bigotimes_{i \in I} |i, s\rangle \langle n_i + \Delta n_i|_{i, z} \langle n_i| \hat{U} |0\rangle_{\omega}. \quad (23)$$

The summation over the photon numbers n_i of the z -polarized modes in Eq. (22) is necessary because EOS is a (partially) nonselective measurement. It is only selective with respect to the photon-number differences between the s - and z -polarized output channels, but not with respect to the actual photon numbers in each polarization. Using again the approximation of the Skellam distribution as already done for the count-probability distribution (see Appendix C for details), the (s_X, s_Y) -parametrized postmeasurement quasiprobability distribution

$$\begin{aligned} \rho'(z; s_X, s_Y) &= \frac{1}{\pi^2} \int e^{z\gamma^* - z^*\gamma} \exp\left(\frac{1+s_Y}{2} \text{Re}^2(\gamma) + \frac{1+s_X}{2} \text{Im}^2(\gamma)\right) \chi'(\gamma; -1) d^2\gamma \\ &\approx N'(z; s_X, s_Y) \rho(z'; s'_X, s'_Y), \end{aligned} \quad (24)$$

with $s_Q < 2\mu^2/(1+A_Q) - 1$ and $Q = X, Y$, is given by the (s'_X, s'_Y) -parametrized quasiprobability distribution of the initial state $\hat{\rho}_{\Omega}$ and a renormalization envelope

$$\begin{aligned} N'(z; s'_X, s'_Y) &= \frac{\sqrt{1-s'_X} \sqrt{1-s'_Y}}{2} \left(\prod_{i \in I} \frac{e^{-\Delta n_i^2/(2|\beta_i|^2)}}{\sqrt{2\pi|\beta_i|^2}} \right) \\ &\times \left[\mu^2 \sqrt{\frac{\mu^2}{1+A_X} - \frac{1+s_X}{2}} \right. \\ &\times \left. \sqrt{\frac{\mu^2}{1+A_Y} - \frac{1+s_Y}{2}} p(\{\Delta n_i\}) \right]^{-1} \\ &\times \exp \left\{ \frac{2 \text{Re}^2[z'(z)]}{1-s'_X} + \frac{2 \text{Im}^2[z'(z)]}{1-s'_Y} + |\tilde{z}|^2 \right. \\ &- \text{Re}^2(z - \tilde{z}) \left(\frac{\mu^2}{1+A_X} - \frac{1+s_X}{2} \right)^{-1} \\ &\left. - \text{Im}^2(z - \tilde{z}) \left(\frac{\mu^2}{1+A_Y} - \frac{1+s_Y}{2} \right)^{-1} \right\}. \end{aligned} \quad (25)$$

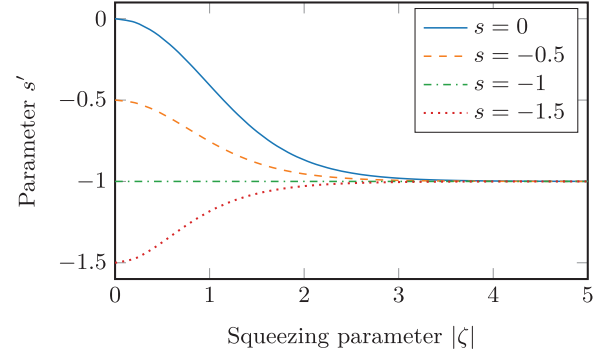


FIG. 4. Parameter $s' = s'_X = s'_Y$ of Eq. (24) for a setup with $A_X = A_Y$ as a function of the squeezing strength $|\zeta|$ for different parameters of the postmeasurement quasiprobability distribution $s = s_X = s_Y$. Among these are the Wigner function with $s = 0$ and the Husimi function with $s = -1$.

Note that this envelope is different from the one in Eq. (13). The parameters of the pre-measurement distribution are

$$s'_Q = 1 - 2\mu^2 \left[|v|^2 + \left(\frac{\mu^2}{1+A_Q} - \frac{1+s_Q}{2} \right)^{-1} \right]^{-1}. \quad (26)$$

The parameters s_Q can be freely chosen [as long as $s_Q < 2\mu^2/(1+A_Q) - 1$ is fulfilled] and are not related to \tilde{s}_Q from Sec. III. The restrictions on the s_Q are necessary to ensure convergence of all integrals. Furthermore, the argument of the quasiprobability distribution ρ of the initial state in Eq. (24) is rescaled and displaced according to

$$\begin{aligned} z'(z) &= \frac{1-s'_X}{2\mu} \text{Re} \left(\tilde{z} + \frac{z - \tilde{z}}{\mu^2/(1+A_X) - (1+s_X)/2} \right) \\ &+ i \frac{1-s'_Y}{2\mu} \text{Im} \left(\tilde{z} + \frac{z - \tilde{z}}{\mu^2/(1+A_Y) - (1+s_Y)/2} \right), \end{aligned} \quad (27)$$

where the displacement is related to the measurement outcomes $\{\Delta n_i\}$ through $\tilde{z} = \frac{|v|}{\mu} \tilde{y}$ with

$$\tilde{y} = \sum_{i_X \in I_X} \frac{|\tilde{\alpha}_{i_X}|}{|\beta_{i_X}|} \Delta n_{i_X} + i \sum_{i_Y \in I_Y} \frac{|\tilde{\alpha}_{i_Y}|}{|\beta_{i_Y}|} \Delta n_{i_Y}. \quad (28)$$

For a configuration with $A_X = A_Y$ the parameter $s' = s'_X = s'_Y$ is shown in Fig. 4 as a function of the squeezing strength for different values of the postmeasurement quasiprobability distributions parameter $s = s_X = s_Y$. At the limit of very weak squeezing, s' tends to s -dependent plateaus due to the vanishing coupling between the MIR and the NIR modes. In the limit of strong squeezing, s' tends to -1 independently of the s value of the postmeasurement quasiprobability distribution; this means that the stronger the squeezing is, the more positive the quasiprobability distribution $\rho'(z, s'_X, s'_Y)$ becomes, because it tends towards the Husimi function $\rho(z; s = -1)$.

In fact, for infinite squeezing, the postmeasurement quasiprobability distribution gives

$$\begin{aligned} \lim_{|\zeta| \rightarrow \infty} \rho'(z; 0) &= \frac{2}{\pi} \exp[-2e^{2r} \text{Re}^2(z - \tilde{y}) - 2e^{-2r} \text{Im}^2(z - \tilde{y})] \end{aligned} \quad (29)$$

and corresponds to a displaced squeezed state $|\tilde{y}, r\rangle$ with squeezing parameter $r = \frac{1}{2} \ln(\sum_{i_X \in I_X} |\tilde{\alpha}_{i_X}|^2 / \sum_{i_Y \in I_Y} |\tilde{\alpha}_{i_Y}|^2)$. This happens as a consequence of the monotonic dependence of the ρ broadening on the squeezing parameter: $\lim_{|\zeta| \rightarrow \infty} z'(z) = 0$. For $A_X = A_Y$ in Eq. (29), $r = 0$, resulting in a coherent state. If only \hat{X} (\hat{Y}) measurements are performed, $r \rightarrow \infty$ ($-\infty$) and Eq. (29) describes a \hat{X} - (\hat{Y} -)quadrature eigenstate; in either case, the state defined by Eq. (29) does not explicitly depend on the initial quasiprobability distribution, but it does depend on the measurement outcomes $\{\Delta n_i\}$, which are conditioned by the choice of an initial state. This is in accordance with the results obtained by Arthurs and Kelly for an ideal measurement [8,63] as well as for a weak Arthurs-Kelly measurement [64].

The same reasoning applies for the case of infinitely many consecutive measurements. A consecutive measurement is defined as an EOS of the postmeasurement MIR state using a copy of the setup in Fig. 1. With every consecutive measurement, the argument of the quasiprobability distribution is rescaled by a factor $\mu^{-1}(1-s')/(1-s)$, which is smaller than 1 for $s < 1$ and $|\zeta| > 0$. Thus, in the limit of infinitely many consecutive measurements, the argument of the quasiprobability distribution $z'(z)$ tends to zero and the resulting quasiprobability distribution only depends on the renormalization envelopes. For a series of symmetric \overline{XY} measurements, the final state seems to always tend to a coherent state if the measurement outcomes are not exceedingly small, as can be seen in Fig. 5 for a cat state. This is also known to happen for continuous, weak Arthurs-Kelly measurements of a harmonic oscillator [65] and for a harmonic oscillator weakly coupled to a thermal bath [66].

V. COMPARISON OF DIFFERENT SIMULTANEOUS MEASUREMENTS

As a benchmark, the following problem is considered: Let us assume that the state of the MIR field is already categorized (e.g., squeezed, displaced, thermal, etc.) and can be parametrized with the parameters $\{\lambda_j\}$. If, for example, it is known that the MIR mode is in a coherent state $|\alpha_\Omega\rangle_\Omega$ with an unknown α_Ω , the task would be to determine the parameter $\lambda_1 = \alpha_\Omega$. The probability distribution of these undetermined parameters, $p(\{\lambda_j\}|\{\Delta n_i\})$, can be directly obtained from the count probability $p(\{\Delta n_i\}) = p(\{\Delta n_i\}|\hat{\rho}_\Omega) = p(\{\Delta n_i\}|\{\lambda_j\})$, since the latter is defined as the distribution of conditional probabilities to measure the photon-number difference Δn_i given that the MIR mode is in the state $\hat{\rho}_\Omega$. Hence, the parameter probability distribution can be calculated using Bayes' theorem (see [67] and [68], p. 42)

$$p(\{\lambda_j\}|\{\Delta n_i\}) = \frac{p(\{\Delta n_i\}|\{\lambda_j\})p(\{\lambda_j\})}{\int p(\{\Delta n_i\}|\{\lambda_j\})p(\{\lambda_j\}) \prod_j d\mu_j(\lambda_j)}, \quad (30)$$

where μ_j is an appropriate measure for the parameter λ_j . Since there is no *a priori* information about the parameters $\{\lambda_j\}$, the initial parameter distribution $p(\{\lambda_j\})$ is assumed to be uniform, in accordance with the indifference principle. With this assumption, the parameter distribution can be expressed

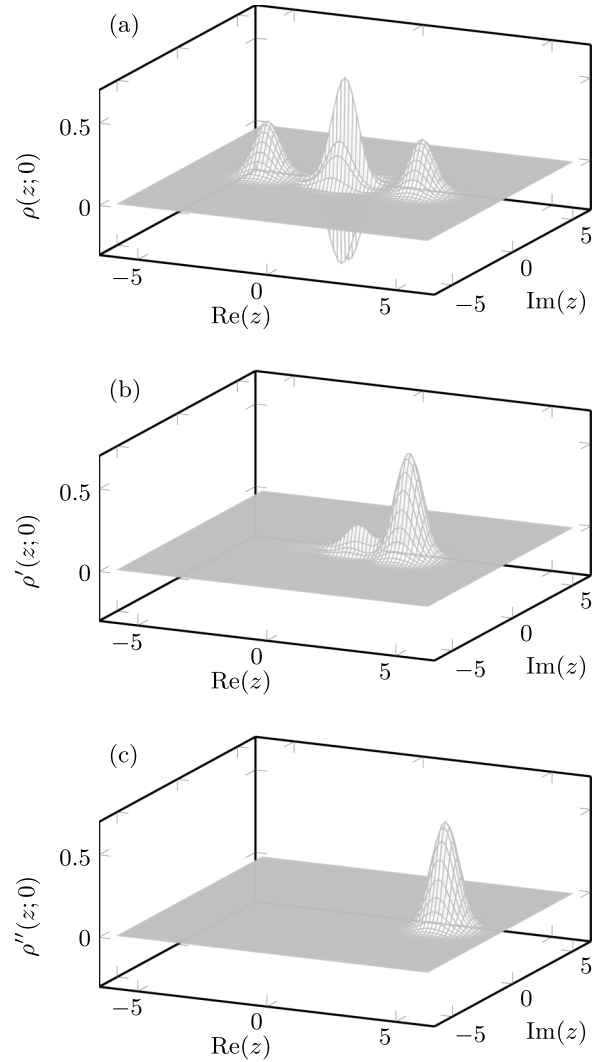


FIG. 5. (a) Wigner function $\rho(z; 0)$ of the cat state proportional to $|\alpha_\Omega\rangle + |-\alpha_\Omega\rangle$ with $\alpha_\Omega = 3$. (b) Wigner function $\rho'(z; 0)$ of the cat state after a symmetric \overline{XY} measurement is performed, with $\zeta = 1$, $\beta_X = \beta_Y = 10$, and measurement outcomes $\Delta n_X = 10$ and $\Delta n_Y = 0$. (c) Wigner function after yet another measurement with the outcomes $\Delta n'_X = 40$ and $\Delta n'_Y = 0$. The outcomes of all measurements are not exceedingly small with $p_1(10, 0) = 0.000\ 012$ and $p_2(40, 0) = 0.000\ 64$.

as

$$p(\{\lambda_j\}|\{\Delta n_i\}) = \frac{\rho(z, \tilde{s}_X, \tilde{s}_Y)}{\int \rho(z, \tilde{s}_X, \tilde{s}_Y) \prod_j d\mu_j(\lambda_j)}. \quad (31)$$

A simple, but for our purposes sufficient, reconstructed state reads [67]

$$\hat{\rho}_{\text{rec}} = \int p(\{\lambda_j\}|\{\Delta n_i\})\hat{\rho}_{(\lambda_j)} \prod_j d\mu_j(\lambda_j), \quad (32)$$

where $\hat{\rho}_{(\lambda_j)}$ is the state parametrized by $\{\lambda_j\}$. For additional measurements, the Bayesian update can be repeated by replacing $p(\{\lambda_j\})$ with $p(\{\lambda_j\}|\{\Delta n_i\})$ as a better estimate of the actual distribution of the parameters (see [68], p. 48). We will denote the count-probability distribution of the first EOS measurement as $p_1(\{\Delta n_i\}|\{\lambda_j\})$. The count-probability

distribution of the second EOS measurement will be denoted by $p_2(\{\Delta n'_i\}|\{\lambda_j\})$, where $\Delta n'_i$ are the measurement outcomes of the second EOS with the NIR frequencies $i' \in I'$. Hence, applying Bayes' law again will update the parameter distribution to

$$p(\{\lambda_j\}|\{\Delta n_i\}, \{\Delta n'_i\}) = \frac{p_2(\{\Delta n'_i\}|\{\lambda_j\})p_1(\{\lambda_j\}|\{\Delta n_i\})}{\int p_2(\{\Delta n'_i\}|\{\lambda_j\})p_1(\{\lambda_j\}|\{\Delta n_i\}) \prod_j d\mu_j(\lambda_j)}. \quad (33)$$

The reconstructed state is thus

$$\hat{\rho}_{\text{rec}} = \int p(\{\lambda_j\}|\{\Delta n_i\}, \{\Delta n'_i\}) \hat{\rho}_{(\lambda_j)} \prod_j d\mu_j(\lambda_j). \quad (34)$$

The fidelity $F(\hat{\rho}_\Omega, \hat{\rho}_{\text{rec}})$ can be used to quantify how close the reconstructed state is to the initial state [69]. However, this fidelity depends on the measurement outcomes $\{\Delta n_i\}$. To get a quantity independent of the measurement outcomes, the average fidelity $\langle F(\hat{\rho}_\Omega, \hat{\rho}_{\text{rec}}) \rangle = \sum_{\{\Delta n_i\}} F(\hat{\rho}_\Omega, \hat{\rho}_{\text{rec}}) p(\{\Delta n_i\})$ can be used.

Similarly, the effect of the measurement on the MIR mode is quantified by the fidelity $F(\hat{\rho}_\Omega, \hat{\rho}'_\Omega)$ between the initial and the postmeasurement state. If the initial state is pure, the fidelity

$$F(\hat{\rho}_\Omega, \hat{\rho}'_\Omega) = \pi \int \rho(z; 0) \rho'(z; 0) d^2 z \quad (35)$$

can be expressed using the Wigner function of the initial state $\rho(z; 0)$ and postmeasurement state $\rho'(z; 0)$. Once again, to get a measurement-outcome independent quantity, the average fidelity is considered.

Numerical results for the average fidelities between the initial and the reconstructed states of a symmetric \overline{XY} measurement and a symmetric \overline{XYXY} measurement can be seen in Fig. 6(a), while the corresponding average fidelities between the initial and postmeasurement states is shown in Fig. 6(b). A symmetric \overline{XYXY} measurement is a simultaneous electro-optic measurement of two \hat{X} quadratures and two \hat{Y} quadratures with equal combined pump strength for both observables, $A_X = A_Y$. The initial states are considered to be the vacuum, a coherent state with $\alpha_\Omega = 3$, and two Fock states with photon numbers $n_\Omega = 1$ and 3. For the fidelity between an initially coherent state and the reconstructed state, an approximate analytical solution has also been derived (cf. Appendix D). The fidelities between initial and reconstructed states obtained from electro-optic sampling converge in the limit of infinitely strong squeezing to the fidelities corresponding to eight-port homodyne detection. This agrees with the limit $\lim_{|\zeta| \rightarrow \infty} \tilde{s} = -1$ discussed in Sec. III. The same holds for the symmetric \overline{XYXY} measurement. In fact, the fidelities of the two measurement schemes coincide for the coherent states. For the Fock states there is a small deviation, not enough to overcome the limit set by eight-port homodyne detection; this happens because the renormalization envelope (13) restricts the pair $(\Delta n_{X_1}, \Delta n_{Y_1})$ of one \overline{XY} measurement to an area close the pair $(\Delta n_{X_2}, \Delta n_{Y_2})$ of the other \overline{XY} measurements. This agrees with the results obtained by Braunstein *et al.* [70]. The small deviation could originate from the fact that the quasiprobability distribution is only sampled discretely and thus different $z(\{\Delta n_i\})$ could lead to different

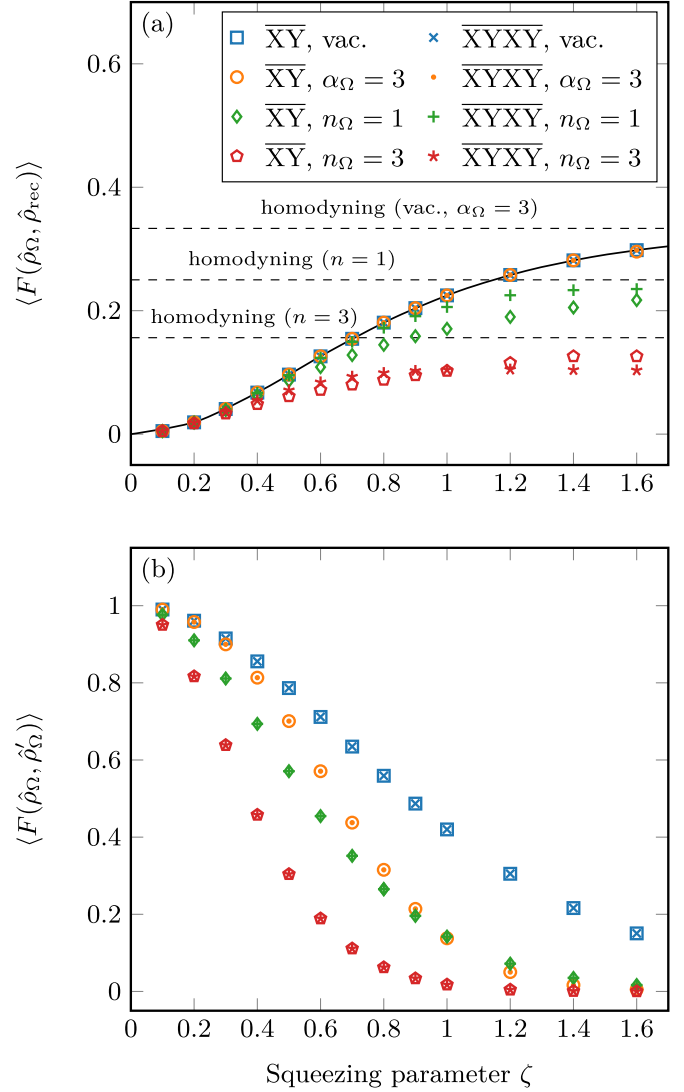


FIG. 6. (a) Numerical evaluation of the average fidelity between the initial MIR state and the reconstructed state in Eq. (32) for various squeezing parameters. The initial state was assumed to be the vacuum, a coherent state with $\alpha_\Omega = 3$, and two Fock states with $n_\Omega = 1$ as well as $n_\Omega = 3$ photons. Also two different measurement setups were considered: a symmetric \overline{XY} measurement and a symmetric \overline{XYXY} measurement. The dashed horizontal lines indicate the fidelity if eight-port homodyne detection would be used in place of electro-optic sampling. The solid line is the approximate solution from Appendix D. (b) Average fidelity between the initial and the postmeasurement state of the MIR field. The initial states are the same as in (a).

fidelities. If one realized an \overline{XYXY} measurement using beam splitters, the minimal number of optical components (without filtering) would be greater than for electro-optic sampling, because the nonlinear interaction is inherently multimode. For an \overline{XY} measurement, the minimal number of optical components is the same for both setups. As a general trend, the fidelities between the initial and the postmeasurement states are close to one for small squeezing and drop to zero for stronger squeezing, as expected because stronger measurements tend to disturb the measured state to a higher extent.

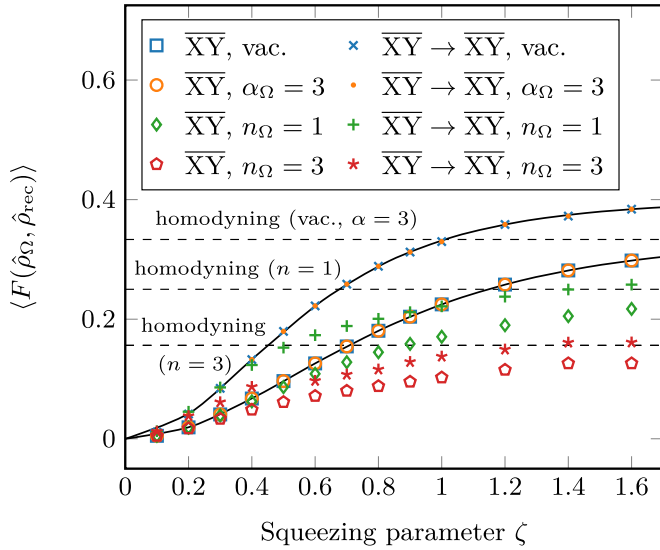


FIG. 7. Numerical evaluation of the average fidelity between the initial and the reconstructed state for various squeezing parameters. The initial state was assumed to be the vacuum, a coherent state with $\alpha_\Omega = 3$, and two Fock states with $n_\Omega = 1$ as well as $n_\Omega = 3$ photons. Also two different measurement setups were considered: a symmetric \overline{XY} measurement and a consecutive measurement $\overline{XY} \rightarrow \overline{XY}$ (a second \overline{XY} electro-optic measurement on the postmeasurement state). The dashed horizontal lines indicate the fidelity if eight-port homodyne detection would be used in place of electro-optic sampling. The solid lines represent the approximate solution from Appendix D.

Furthermore, the fidelities for Fock states drop faster than the ones for coherent states.

There is another way to obtain two \hat{X} - and two \hat{Y} -quadrature measurements. First a symmetric \overline{XY} measurement is performed and then the same measurement is done on the postmeasurement state of the first EOS (i.e., a consecutive measurement). We will denote this by $\overline{XY} \rightarrow \overline{XY}$. To obtain the parameter distribution, and therewith the fidelity corresponding to the reconstructed state, the Bayesian update has to be initially performed with the probability distribution of the first measurement $p_1(\{\Delta n_i\}|\{\lambda_j\})$ and then again with the probability distribution of the second measurement $p_2(\{\Delta n'_i\}|\{\lambda_j\})$, resulting in Eq. (33). A numerical evaluation of these fidelities can be seen in Fig. 7. One can see that the fidelities between the initial and the reconstructed states exceed the limits set by eight-port homodyne detection. Thus, eight-port homodyne detection is not optimal and can, at least in principle, be outperformed by our proposed measurement scheme based on electro-optic sampling. The experimental implementation of consecutive measurements is of course more complex and thus might diminish the advantage, which could be offset by further optimization. To conclusively quantify the advantage under realistic conditions, further analysis is needed. For an \overline{XY} measurement of a coherent state, the asymptote of the approximate solution is $\frac{1}{3}$, while for the consecutive case it improves to $\frac{2}{5}$. This asymptotic behavior might appear to be inconsistent with the postmeasurement state in the strong squeezing limit [Eq. (29)] since the quasiprobability distribution after the measurement

seems to be independent of the initial state; however, while the postmeasurement quasiprobability distribution does not depend on the quasiprobability distribution of the initial state, it does depend on the outcomes $\{\Delta n_i\}$ of the first measurement, which are conditioned to the initial state and its phase-space representations. Hence, the $\zeta \rightarrow \infty$ postmeasurement state is not completely independent of the initial state and allows the consecutive-measurement fidelity between the initial and the reconstructed states to exceed the limit of an \overline{XY} measurement.

VI. CONCLUSION

Considering the recent progress in quantum electro-optic sampling of the quantum vacuum and squeezed vacuum [34,36,39,65,71], we proposed a quantum tomography scheme based on continuous-wave driven electro-optic sampling, paving the way towards tomography of ultrabroadband quantum states in the time domain. In this work, we proposed a multichannel version of electro-optic sampling involving monochromatic modes and described such measurements within the framework of the POVM formalism. In this scheme, the MIR mode interacts with multiple NIR pump modes, allowing for arbitrary combinations of \hat{X} - and/or \hat{Y} -quadrature measurements. The count-probability distribution was shown to be determined by a quasiprobability distribution together with a renormalization envelope. The parameters \tilde{s}_X and \tilde{s}_Y of this quasiprobability distribution only depend on the parameters associated with the nonlinear interaction. These parameters \tilde{s}_X and \tilde{s}_Y , and thus the nonlinear interaction, determine an extra noise term on top of the quadrature variances (i.e., the shot noise), while the probe only rescales the distribution. If only \hat{X} (\hat{Y}) measurements are performed, the count probability is related to the Weierstrass transform of the quantum-mechanical quadrature distribution $\langle x|\hat{\rho}_\Omega|x\rangle$ ($\langle y|\hat{\rho}_\Omega|y\rangle$).

For the postmeasurement quasiprobability distributions, the effect of the measurement is a change in the quasiprobability distributions parameters, a renormalization and shift of both the quasiprobability distribution and its argument. In the limit case of an infinitely strong nonlinear interaction, the quasiprobability distribution represents a displaced squeezed state; if the sum of all NIR pump amplitudes of the \hat{X} measurements equals that of all \hat{Y} measurements, it represents a coherent state, while the postmeasurement state is squeezed into a quadrature eigenstate as either the \hat{X} or \hat{Y} quadrature measurements prevail over the other.

Finally, we compared several variants of multichannel electro-optic sampling with the well-established eight-port homodyne detection. No significant difference was found between the \overline{XY} measurement and the (simultaneous) \overline{XYXY} measurement. This can be explained by correlations between the first \hat{X} and \hat{Y} pair and the second one. In the limit of infinite squeezing, the fidelity between the reconstructed state and the initial MIR state asymptotically tends to the value set by eight-port homodyne detection. Nevertheless, the multichannel EOS can exceed this limit and therefore eight-port homodyne measurements by using two consecutive measurements of both quadratures, as we showed for a diverse selection of quantum states (see Fig. 7).

The fidelity between the initial and reconstructed states could potentially be further optimized by varying all the parameters allowed by the present description. For example, a consecutive measurement with different squeezing strengths for each measurement could be considered, to minimize the measurement backaction. Additionally, the fidelity could be improved by simultaneously measuring an additional intermediate quadrature different from the \hat{X} or the \hat{Y} quadratures.

The main significance of our results lies in the insight that eight-port homodyne measurements are not necessarily optimal for optical quantum tomography and can be outperformed by our proposed measurement scheme based on electro-optic sampling. Furthermore, we have provided a concrete realization of an Arthurs-Kelly measurement at arbitrary interaction strengths between the system and detectors. On the theoretical side, we have developed a formalism based on POVMs to describe the count-probability distribution and the postmeasurement state in phase space.

ACKNOWLEDGMENTS

We acknowledge funding from the Deutsche Forschungsgemeinschaft Project No. 425217212, SFB 1432. T.L.M.G. gratefully acknowledges funding from the Baden-Württemberg Stiftung via the Elite Programme for Postdocs.

APPENDIX A: COUNT-PROBABILITY DISTRIBUTION

In this Appendix we will use an alternative representation for the action of the waveplate on the NIR mode i using the matrix notation

$$\hat{U}_{i,\text{WP}} \begin{pmatrix} \hat{a}_{i,s} \\ \hat{a}_{i,z} \end{pmatrix} \hat{U}_{i,\text{WP}}^\dagger = e^{-i\phi_i/2} \begin{pmatrix} (W_i)_{11} & (W_i)_{12} \\ (W_i)_{21} & (W_i)_{22} \end{pmatrix} \begin{pmatrix} \hat{a}_{i,s} \\ \hat{a}_{i,z} \end{pmatrix}, \quad (\text{A1})$$

with the matrix elements

$$(W_i)_{11} = (W_i)_{22}^* = \cos(\phi_i/2) + i \sin(\phi_i/2) \cos(2\theta_i), \quad (\text{A2})$$

$$(W_i)_{12} = (W_i)_{21} = i \sin(\phi_i/2) \sin(2\theta_i). \quad (\text{A3})$$

Starting from Eq. (5) and using the Glauber-Sudarshan distributions $\rho_{n_i+\Delta n_i}(\eta_{i,s}; 1)$ and $\rho_{n_i}(\eta_{i,z}; 1)$ for the Fock states $|n_i + \Delta n_i\rangle_{i,s}$ and $|n_i\rangle_{i,z}$,

$$\hat{P}_{\Delta n_i} = \iint \sum_{n_i=\bar{n}_i}^{\infty} \rho_{n_i+\Delta n_i}(\eta_{i,s}; 1) \rho_{n_i}(\eta_{i,z}; 1) \times |\eta_{i,s}\rangle_{i,s} \langle \eta_{i,s}| \otimes |\eta_{i,z}\rangle_{i,z} \langle \eta_{i,z}| d^2\eta_{i,s} d^2\eta_{i,z}, \quad (\text{A4})$$

as well as for the MIR state [Eq. (6)], we can express the count-probability distribution as a convolution of the Glauber-Sudarshan distributions with some matrix elements of the time-evolution operator,

$$p(\{\Delta n_i\}) = \prod_{i \in I} \sum_{n_i=\bar{n}_i}^{\infty} \iiint \rho(\gamma; 1) \rho_{n_i+\Delta n_i}(\eta_{i,s}; 1) \times \rho_{n_i}(\eta_{i,z}; 1) |\Omega \langle \gamma' |_{i,s} \langle \eta_{i,s} |_{i,z} \langle \eta_{i,z} | \hat{U} | 0 \rangle_{i,z} | 0 \rangle_{i,s} \times |\gamma \rangle_{\Omega} |^2 d^2\gamma d^2\gamma' d^2\eta_{i,s} d^2\eta_{i,z}. \quad (\text{A5})$$

We rewrite the total time-evolution operator defined by Eq. (2) as

$$\hat{U} = \hat{U}_{\text{WP}} \hat{D}_z(\vec{\beta}) \hat{U}_{\text{NL}} \\ = \hat{U}_{\text{WP}} \hat{D}_z(\vec{\beta}) \hat{U}_{\text{WP}}^\dagger \hat{U}_{\text{WP}} \hat{U}_{\text{NL}} \hat{U}_{\text{WP}}^\dagger \hat{U}_{\text{WP}}. \quad (\text{A6})$$

This can later be simplified using $\hat{U}_{\text{WP}}|0\rangle_{\omega} = |0\rangle_{\omega}$, with the vacuum NIR state $|0\rangle_{\omega} = \bigotimes_{i \in I} |0\rangle_{i,s} |0\rangle_{i,z}$, and

$$\hat{U}_{\text{WP}} \hat{D}_{i,z}(\beta_i) \hat{U}_{\text{WP}}^\dagger \\ = \hat{D}_{i,s}[(W_i^{-1})_{21}^* \beta_i] \otimes \hat{D}_{i,z}[(W_i^{-1})_{22}^* \beta_i]. \quad (\text{A7})$$

The squeezing operator can also be simplified. First, we decompose it using $\mu = \cosh(|\zeta|)$ and $\nu = \frac{\zeta}{|\zeta|} \sinh(|\zeta|)$ (see [18], p. 100):

$$\hat{U}_{\text{NL}} = \exp\left(\zeta^* \hat{a}_{\Omega,s} \sum_{i \in I} \tilde{\alpha}_i \hat{a}_{i,s} - \text{H.c.}\right) \\ = \exp\left(-\frac{\nu}{\mu} \hat{a}_{\Omega,s}^\dagger \sum_{i \in I} \tilde{\alpha}_i^* \hat{a}_{i,s}^\dagger\right) \\ \times \left(\frac{1}{\mu}\right)^{\hat{a}_{\Omega,s}^\dagger \hat{a}_{\Omega,s} + (\sum_{i \in I} \tilde{\alpha}_i \hat{a}_{i,s})^\dagger \sum_{i \in I} \tilde{\alpha}_i \hat{a}_{i,s} + 1} \\ \times \exp\left(\frac{\nu^*}{\mu} \hat{a}_{\Omega,s} \sum_{i \in I} \tilde{\alpha}_i \hat{a}_{i,s}\right). \quad (\text{A8})$$

Now all terms with $\hat{a}_{i,s}|0\rangle_{\omega} = 0$ or $\hat{a}_{i,z}|0\rangle_{\omega} = 0$ vanish when applied to the vacuum:

$$\hat{U}_{\text{NL}}|0\rangle_{\omega} = \exp\left(-\frac{\nu}{\mu} \hat{a}_{\Omega,s}^\dagger \sum_{i \in I} \tilde{\alpha}_i^* \hat{a}_{i,s}^\dagger\right) \left(\frac{1}{\mu}\right)^{\hat{a}_{\Omega,s}^\dagger \hat{a}_{\Omega,s} + 1} |0\rangle_{\omega}. \quad (\text{A9})$$

Finally, the matrix elements of the total time-evolution operator (2) in the coherent-state basis, using $|\eta\rangle_{\omega} = \bigotimes_{i \in I} |\eta_{i,s}\rangle_{i,s} |\eta_{i,z}\rangle_{i,z}$, can be calculated:

$$\Omega \langle \gamma' |_{\omega} \langle \eta | \hat{U} | 0 \rangle_{\omega} | \gamma \rangle_{\Omega} \\ = \frac{1}{\mu} e^{-|\gamma|^2/2 - |\gamma'|^2/2 + \gamma(\gamma')^*/\mu} \left\{ \prod_i \right. \\ \times {}_{i,s} \langle \eta_{i,s} | \hat{D}_{i,s}[(W_i^{-1})_{21}^* \beta_i] e^{-(\nu/\mu) \tilde{\alpha}_i^* (\gamma')^* (W_i^{-1})_{11}^* \hat{a}_{i,s}} | 0 \rangle_{i,s} \\ \times {}_{i,z} \langle \eta_{i,z} | \hat{D}_{i,z}[(W_i^{-1})_{22}^* \beta_i] e^{-(\nu/\mu) \tilde{\alpha}_i^* (\gamma')^* (W_i^{-1})_{12}^* \hat{a}_{i,z}} | 0 \rangle_{i,z} \left. \right\} \\ = e^{\sum_i -(\nu/\mu) \tilde{\alpha}_i^* (\gamma')^* (W_i^{-1})_{11}^* (\eta_{i,s} - (W_i^{-1})_{21}^* \beta_i) - |\eta_{i,s} - (W_i^{-1})_{21}^* \beta_i|^2/2} \\ \times e^{\sum_i -(\nu/\mu) \tilde{\alpha}_i^* (\gamma')^* (W_i^{-1})_{12}^* (\eta_{i,z} - (W_i^{-1})_{22}^* \beta_i) - |\eta_{i,z} - (W_i^{-1})_{22}^* \beta_i|^2/2} \\ \times \frac{1}{\mu} e^{-|\gamma|^2/2 - |\gamma'|^2/2 + \gamma(\gamma')^*/\mu} \\ = e^{-(\nu/\mu) \tilde{\alpha}_i^* (W_i)_{11} (\gamma')^* \eta_{i,s}^* - |\eta_{i,s} - (W_i)_{21} \beta_i|^2/2} \\ \times e^{-(\nu/\mu) \tilde{\alpha}_i^* (W_i)_{12} (\gamma')^* \eta_{i,z}^* - |\eta_{i,z} - (W_i)_{22} \beta_i|^2/2} \\ \times \frac{1}{\mu} \exp[-|\gamma|^2/2 - |\gamma'|^2/2 + \gamma(\gamma')^*/\mu]. \quad (\text{A10})$$

In the last equality, we used $(W_i^{-1})_{11}^*(W_i^{-1})_{21} + (W_i^{-1})_{12}^*(W_i^{-1})_{22} = 0$. Since the matrix elements are Gaussian functions, the convolutions give the Weierstrass transforms of $\rho_{n_i+\Delta n_i}(\eta_{i,s}; 1)$ and $\rho_{\Delta n_i}(\eta_{i,z}; 1)$ [i.e., the Husimi function $\rho_{n_i+\Delta n_i}(\sqrt{\tilde{m}_{i,1}}; -1)$ and $\rho_{n_i}(\sqrt{\tilde{m}_{i,2}}; -1)$]. The count distribution can thus be written as

$$p(\{\Delta n_i\}) = \frac{\pi}{\mu^2} \exp\left(-\sum_{i \in I} |\beta_i|^2\right) \int \rho(\gamma; 1) e^{-|\gamma|^2} \int \exp\left(-|\gamma'|^2 + \frac{2}{\mu} \text{Re}(\gamma' \gamma^*) + \sum_{i \in I} \tilde{m}_{i,1} + \tilde{m}_{i,2}\right) \\ \times \prod_{i \in I} \sum_{n_i=\tilde{n}_i}^{\infty} \rho_{n_i+\Delta n_i}(\sqrt{\tilde{m}_{i,1}}; -1) \rho_{n_i}(\sqrt{\tilde{m}_{i,2}}; -1) d^2 \gamma' d^2 \gamma, \quad (\text{A11})$$

with

$$\tilde{m}_{i,j} = \left| (W_i)_{2j}^* \beta_i - \frac{\nu}{\mu} \tilde{\alpha}_i^* (W_i)_{1j} (\gamma')^* \right|^2. \quad (\text{A12})$$

The last line in Eq. (A11) can be expressed using the Skellam distribution [72]

$$p_s(\Delta n_i; \tilde{m}_{i,1}, \tilde{m}_{i,2}) = \sum_{n_i=\tilde{n}_i}^{\infty} \rho_{n_i+\Delta n_i}(\sqrt{\tilde{m}_{i,1}}; -1) \rho_{n_i}(\sqrt{\tilde{m}_{i,2}}; -1) \\ = e^{-(\tilde{m}_{i,1}+\tilde{m}_{i,2})} \left(\frac{\tilde{m}_{i,1}}{\tilde{m}_{i,2}}\right)^{\Delta n_i/2} I_{\Delta n_i}(2\sqrt{\tilde{m}_{i,1}\tilde{m}_{i,2}}), \quad (\text{A13})$$

with the modified Bessel function I , which is the probability distribution of the difference Δn_i between two Poissonian counting events with expectation values $\tilde{m}_{i,1}$ and $\tilde{m}_{i,2}$.

To get a balanced signal (as described in the main text), the expectation value $\tilde{m}_{i,1} - \tilde{m}_{i,2}$ of the argument of the Skellam distribution has to be proportional to γ' [terms proportional to $|\beta_i|^2$ would lead to a shift of Δn_i , as will become clear from Eqs. (A17) and (A19) later]. All the unwanted terms cancel if the matrix elements describing the effect of the waveplates are restricted to $(W_i)_{11}/(W_i)_{21} = -(W_i)_{12}/(W_i)_{22}$, leading to Eq. (7). For $\frac{\pi}{2} \leq \phi_i \leq \frac{3}{2}\pi$, the fraction

$$\frac{(W_i)_{11}}{(W_i)_{21}} = (-1)^{k_1+k_2} \left[\sqrt{-\cos(\phi_i)} - (-1)^{k_2} i \sqrt{2} \cos\left(\frac{\phi_i}{2}\right) \right] \\ = \exp\{(-1)^{k_2} i \arcsin[\sqrt{2} \cos(\phi_i/2)] + i\pi[k_1 + k_2 + 1]\} \quad (\text{A14})$$

is a complex phase [because $|(W_i)_{21}(W_i)_{22}| = \frac{1}{2}$ and $|(W_i)_{21}|/|(W_i)_{22}| = 1$] and the count-probability distribution can be expressed as

$$p(\{\Delta n_i\}) = \frac{\pi}{\mu^2} \exp\left(-\sum_{i \in I} |\beta_i|^2\right) \int \rho(\gamma; 1) e^{-|\gamma|^2} \int \exp\left(-|\gamma'|^2 + \frac{2}{\mu} \text{Re}(\gamma' \gamma^*) + \sum_{i \in I} m_{i,1} + m_{i,2}\right) \\ \times \prod_{i \in I} p_s(\Delta n_i; m_{i,1}, m_{i,2}) d^2 \gamma' d^2 \gamma, \quad (\text{A15})$$

with

$$m_{i,j} = \frac{1}{2} \left| |\beta_i| + (-1)^{j-1} e^{i\phi_i} \frac{|\nu|}{\mu} |\tilde{\alpha}_i| (\gamma')^* \right|^2. \quad (\text{A16})$$

The expectation values of the arguments of the Skellam distributions $p_s(\Delta n_i; m_{i,1}, m_{i,2})$ [73],

$$m_{i,1} - m_{i,2} = 2 \frac{|\nu|}{\mu} |\tilde{\alpha}_i| |\beta_i| \text{Re}[e^{i\phi_i} (\gamma')^*], \quad (\text{A17})$$

are proportional to γ' . The variances

$$m_{i,1} + m_{i,2} = |\beta_i|^2 + \frac{|\nu|^2}{\mu^2} |\tilde{\alpha}_i|^2 |\gamma'|^2 \approx |\beta_i|^2, \quad (\text{A18})$$

on the other hand, are approximately given by the probe amplitudes. The latter are assumed to be much stronger than the contribution from the nonlinear interaction. Since the variances (A18) are large, the Skellam distributions can be approximated as normal distributions with the same expectation values and variances,

$$p_s(\Delta n_i; m_{i,1}, m_{i,2}) \approx \frac{1}{\sqrt{2\pi} |\beta_i|} e^{-\{\Delta n_i - 2(|\nu|/\mu) |\tilde{\alpha}_i| |\beta_i| \text{Re}[e^{i\phi_i} (\gamma')^*]\}^2 / 2|\beta_i|^2}. \quad (\text{A19})$$

This approximation is derived in Appendix B.

APPENDIX B: SKELLAM DISTRIBUTION

Let us assume that $\rho(\gamma; 1) \approx 0$ for large γ ; thus only small values for γ contribute. Using that $\exp(-|\gamma' - \gamma/\mu|^2) \approx 0$ for large γ' and small γ , we can conclude that only small γ' are relevant and therefore $m_{i,1}$ and $m_{i,2}$ are large if β_i is large, which is the case for strong probe amplitudes. This allows us to approximate the Husimi function by a Gaussian distribution

$$\pi \rho_{n_i+\Delta n_i}(\sqrt{m_{i,1}}; -1) = \frac{|m_{i,1}|^{n_i+\Delta n_i}}{(n_i + \Delta n_i)!} e^{-|m_{i,1}|} \approx \frac{1}{\sqrt{2\pi m_{i,1}}} e^{-(n_i+\Delta n_i-m_{i,1})^2/2m_{i,1}} \quad (\text{B1})$$

$$\pi \rho_{n_i}(\sqrt{m_{i,2}}; -1) = \frac{|m_{i,2}|^{n_i}}{n_i!} e^{-|m_{i,2}|} \approx \frac{1}{\sqrt{2\pi m_{i,2}}} e^{-(n_i-m_{i,2})^2/2m_{i,2}}. \quad (\text{B2})$$

Inserting this in the definition of the Skellam distribution from Eq. (A13), it takes the form

$$\begin{aligned} p_s(\Delta n_i; m_{i,1}, m_{i,2}) &= \pi^2 \sum_{n_i=\bar{n}_i}^{\infty} \rho_{n_i+\Delta n_i}(\sqrt{m_{i,1}}; -1) \rho_{n_i}(\sqrt{m_{i,2}}; -1) \\ &\approx \frac{1}{2\pi \sqrt{m_{i,1} m_{i,2}}} e^{-m_{i,2}/2 - (\Delta n_i - m_{i,1})^2/2m_{i,1}} \vartheta_3\left(\frac{1}{2i\pi}(2 - \Delta n_i/m_{i,1}), -\frac{1}{\pi i} \frac{m_{i,1} + m_{i,2}}{2m_{i,1} m_{i,2}}\right) \\ &= \frac{1}{\sqrt{2\pi(m_{i,1} + m_{i,2})}} e^{-(m_{i,1} - m_{i,2} - \Delta n_i)^2/(2m_{i,1} + 2m_{i,2})} \vartheta_3\left(\frac{(\Delta n_i - 2m_{i,1})m_{i,2}}{m_{i,1} + m_{i,2}}, \pi i \frac{2m_{i,1} m_{i,2}}{m_{i,1} + m_{i,2}}\right), \end{aligned} \quad (\text{B3})$$

where $\vartheta_3(z; \tau) = \sum_{n \in \mathbb{Z}} e^{\pi i n^2 \tau + 2\pi i n z} = 1 + 2 \sum_{n=1}^{\infty} e^{\pi i n^2 \tau} \cos(2\pi n z)$ is the Jacobi theta function. In the last step of Eq. (B3), the identity $\vartheta_3(z; \tau) = \frac{1}{\sqrt{-i\tau}} e^{-\pi i z^2/\tau} \vartheta_3\left(\frac{z}{\tau}; \frac{-1}{\tau}\right)$ was used. This justifies the approximation $\vartheta_3(z; \tau) \approx 1$ of the theta function, because for strong probe amplitudes, the second argument of the theta function is $\tau = \pi i \frac{2m_{i,1} m_{i,2}}{m_{i,1} + m_{i,2}} \sim i|\beta_i|^2$.

APPENDIX C: POSTMEASUREMENT QUASIPROBABILITY DISTRIBUTION

To calculate the (s_X, s_Y) -parametrized quasiprobability distribution, with $s_Q < 2\mu^2/(1 + A_Q) - 1$, the antinormally ordered characteristic function of the postmeasurement state is needed:

$$\chi'(\xi; -1) = \text{tr}(\hat{\rho}'_{\Omega} e^{-\xi^* \hat{a}_{\Omega}} e^{\xi \hat{a}_{\Omega}^{\dagger}}) = \frac{1}{\pi p(\{\Delta n_i\})} \int \rho(\gamma; 1) \int e^{2i \text{Im}[\xi(\gamma')^*]} \sum_{\{n_i\}} |\langle \gamma' | \hat{M}_{\{n_i, \Delta n_i\}} | \gamma \rangle_{\Omega}|^2 d^2 \gamma' d^2 \gamma. \quad (\text{C1})$$

Expressing the Fock states again using the Glauber-Sudarshan distribution, as done in Appendix A, the characteristic function is

$$\begin{aligned} \chi'(\xi; -1) &= \frac{1}{\pi p(\{\Delta n_i\})} \int \rho(\gamma; 1) \int e^{2i \text{Im}[\xi(\gamma')^*]} \sum_{\{n_i\}} \iint |\langle \gamma' |_{i,s} \langle n_{i,s} |_{i,z} \langle n_{i,z} | \hat{U} | 0 \rangle_{i,z} | 0 \rangle_{i,s} | \gamma \rangle_{\Omega}|^2 \\ &\quad \times \rho_{n_i+\Delta n_i}(\eta_{i,s}; 1) \rho_{n_i}(\eta_{i,z}; 1) d^2 \eta_{i,s} d^2 \eta_{i,z} d^2 \gamma' d^2 \gamma. \end{aligned} \quad (\text{C2})$$

The matrix elements are already known from the count-probability distribution and thus the problem can be solved by applying the same approximation of the Skellam distribution as before. With this approximation, the characteristic function is

$$\begin{aligned} \chi'(\xi; -1) &\approx \left(p^2(\{\Delta n_i\})(1 + A_X)(1 + A_Y) \prod_i 2\pi |\beta_i|^2 \right)^{-1/2} \exp\left(-\sum_i \Delta n_i^2 / 2|\beta_i|^2\right) \int \rho(\gamma; 1) \exp\left\{-|\gamma|^2\right. \\ &\quad \left. + \left[\frac{\text{Re}(\gamma)}{\mu} + i \text{Im}(\xi) + \frac{|\nu|}{\mu} \sum_{i \in L_X} \frac{|\tilde{\alpha}_i|}{|\beta_i|} \Delta n_i\right]^2 \frac{\mu^2}{1 + A_X} + \left[\frac{\text{Im}(\gamma)}{\mu} - i \text{Re}(\xi) + \frac{|\nu|}{\mu} \sum_{i \in L_Y} \frac{|\tilde{\alpha}_i|}{|\beta_i|} \Delta n_i\right]^2 \frac{\mu^2}{1 + A_Y}\right\} d^2 \gamma. \end{aligned} \quad (\text{C3})$$

The (s_X, s_Y) -parametrized quasiprobability distribution can then be calculated from the antinormally ordered characteristic function using the Fourier transformation:

$$\begin{aligned} \rho'(z; s_X, s_Y) &= \frac{1}{\pi^2} \int e^{z^* \xi^* - z^* \xi} \exp\left(\frac{1 + s_Y}{2} \text{Re}^2(\xi) + \frac{1 + s_X}{2} \text{Im}^2(\xi)\right) \chi'(\xi; -1) d\xi \\ &\approx N'(z; s_X, s_Y) \rho(z'(z); s'_X, s'_Y). \end{aligned} \quad (\text{C4})$$

This is also where the restrictions $s_Q < 2\mu^2/(1 + A_Q) - 1$ originate from, because only for those values do the integrals in the above equation converge.

APPENDIX D: APPROXIMATION OF THE FIDELITY

Since the coherent states $|\alpha_\Omega\rangle$ are overcomplete $\int \rho_{\alpha_\Omega}(z; s_X, s_Y) d^2\alpha_\Omega = 1$, the parameter distribution is just

$$p(\alpha_\Omega|\{\Delta n_i\}) = \rho_{\alpha_\Omega}(z; s_X, s_Y) \quad (\text{D1})$$

and hence the reconstructed state is

$$\hat{\rho}_{\text{rec}} = \int \rho_{\alpha_\Omega}(z; s_X, s_Y) |\alpha_\Omega\rangle_\Omega \langle \alpha_\Omega| d^2\alpha_\Omega. \quad (\text{D2})$$

Now we can calculate the fidelity between the initial and reconstructed states

$$\begin{aligned} F(\hat{\rho}_\Omega, \hat{\rho}_{\text{rec}}) &= \int \rho_{\alpha_\Omega}(z; s_X, s_Y) |\langle \alpha|\alpha_\Omega\rangle|^2 d^2\alpha_\Omega \\ &= 2 \frac{\sqrt{(1-s_X)(1-s_Y)}}{\sqrt{[2/(1-s_X)+1][2/(1-s_Y)+1]}} \exp\left[\text{Re}^2\left(\frac{2}{1-s_X}z + \alpha_\Omega\right) / \left(\frac{2}{1-s_X} + 1\right)\right] \\ &\quad + \text{Im}^2\left(\frac{2}{1-s_Y}z + \alpha_\Omega\right) / \left(\frac{2}{1-s_Y} + 1\right) - \frac{2}{1-s_X}\text{Re}^2(z) - \frac{2}{1-s_Y}\text{Im}^2(z) - |\alpha_\Omega|^2]. \end{aligned} \quad (\text{D3})$$

To calculate the average fidelity between the initial and reconstructed states, the same approximation for the sum as in Sec. III A is applied. Using this approximation, the average fidelity for a \overline{XY} measurement, as well as for a \overline{XYXY} measurements of a coherent state $|\alpha_\Omega\rangle_\Omega$, is

$$\langle F(\hat{\rho}_\Omega, \hat{\rho}_{\text{rec}}) \rangle = \sum_{\Delta n_X, \Delta n_Y} p(\Delta n_X, \Delta n_Y) F(\hat{\rho}_\Omega, \hat{\rho}_{\text{rec}}) \approx \pi \int \rho_{\alpha_\Omega}(z; s) F(\hat{\rho}_\Omega, \hat{\rho}_{\text{rec}}) d^2z = \frac{1}{\pi} \frac{1}{s-2} = [2 \coth^2(|\zeta|) + 1]^{-1}, \quad (\text{D4})$$

which can be seen in Fig. 6(a) as a function of the squeezing $|\zeta|$. The limit of this function for $|\zeta| \rightarrow \infty$ is $\frac{1}{3}$.

For consecutive $\overline{XY} \rightarrow \overline{XY}$ measurements of a coherent state $|\alpha_\Omega\rangle_\Omega$ the parameter distribution is

$$p(\alpha|\{\Delta n_i\}, \{\Delta n'_i\}) = \frac{\rho_{\alpha_\Omega}(z; s_X, s_Y) \rho_{\alpha_\Omega}(z'; s'_X, s'_Y)}{\int \rho_{\alpha_\Omega}(z; s_X, s_Y) \rho_{\alpha_\Omega}(z'; s'_X, s'_Y) d^2\alpha_\Omega}, \quad (\text{D5})$$

with

$$\begin{aligned} \int \rho_{\alpha_\Omega}(z; s_X, s_Y) \rho_{\alpha_\Omega}(z'; s'_X, s'_Y) d^2\alpha_\Omega &= \frac{1}{\pi} \frac{(1-s)(1-s')}{2/(1-s) + 2/(1-s')} \exp\left(\left|\frac{2}{1-s}z + \frac{2}{1-s'}z'\right|^2\right) \\ &\quad \times \left(\frac{2}{1-s} + \frac{2}{1-s'}\right)^{-1} - \frac{2|z|^2}{1-s} - \frac{2|z'|^2}{1-s'}. \end{aligned} \quad (\text{D6})$$

The fidelity for consecutive $\overline{XY} \rightarrow \overline{XY}$ measurements of a coherent state $|\alpha_\Omega\rangle_\Omega$ is therefore

$$\begin{aligned} F(\hat{\rho}_\Omega, \hat{\rho}_{\text{rec}}) &= \frac{\int \rho_{\alpha_\Omega}(z; s) \rho_{\alpha_\Omega}(z'; s) |\langle \alpha|\alpha_\Omega\rangle|^2 d^2\alpha}{\int \rho_{\alpha_\Omega}(z; s_X, s_Y) \rho_{\alpha_\Omega}(z'; s'_X, s'_Y) d^2\alpha_\Omega} \\ &= \left(\frac{2}{1-s} + \frac{2}{1-s'}\right) \left(\frac{2}{1-s} + \frac{2}{1-s'} + 1\right)^{-1} e^{|\alpha_\Omega|^2} \\ &\quad \times \exp\left[\left|\frac{2}{1-s}z + \frac{2}{1-s'}z'\right|^2 \left(\frac{2}{1-s} + \frac{2}{1-s'}\right)^{-1}\right. \\ &\quad \left. + \left|\frac{2}{1-s}z + \frac{2}{1-s'}z' + \alpha_\Omega\right|^2 \left(\frac{2}{1-s} + \frac{2}{1-s'} + 1\right)^{-1}\right]. \end{aligned} \quad (\text{D7})$$

The average fidelity can then be obtained using the same approximation as for the single EOS measurement [$z_1 = \frac{1}{\sqrt{2|\nu||\beta|}}(\Delta n_X + i\Delta n_Y)$ and $z_2 = \frac{1}{\sqrt{2|\nu||\beta|}}(\Delta n'_X + i\Delta n'_Y)$]:

$$\begin{aligned} \langle F(\hat{\rho}_\Omega, \hat{\rho}_{\text{rec}}) \rangle &= \sum_{\Delta n_X, \Delta n_Y, \Delta n'_X, \Delta n'_Y} p_1(\Delta n_X, \Delta n_Y) p_2(\Delta n'_X, \Delta n'_Y) F(\hat{\rho}_\Omega, \hat{\rho}_{\text{rec}}) \approx \frac{4\pi^2|\beta|^4|\nu|^4}{4\pi|\beta|^4|\nu|^2} \frac{1}{\pi^2} \frac{|\nu|^4}{\mu^4} \frac{1}{|\nu|^2/\mu^2 + 1} \\ &\quad \times \iint \exp\left(-|\nu|^2(|z_1|^2 + |z_2|^2 - |z_1 + z_2|^2/2) - \frac{|\nu|^2}{\mu^2} |\alpha_\Omega - (z_1 + z_2)/\sqrt{2}|^2 - \frac{|\nu|^2}{2\mu^2} |z_1 + z_2|^2 - |\alpha_\Omega|^2\right) \end{aligned}$$

$$\begin{aligned}
& + |\alpha_\Omega - \frac{|v|^2}{\mu^2} (z_1 + z_2)/\sqrt{2}|^2 (|v|^2/\mu^2 + 1)^{-1} \Big) d^2 z_1 d^2 z_2 \\
& = \frac{1}{\pi} \frac{\sinh^2(|\zeta|)}{2 \cosh^6(|\zeta|)} \left[1 + \sinh^2(|\zeta|) + \frac{1}{2} \sinh^4(|\zeta|) \right]. \tag{D8}
\end{aligned}$$

See Fig. 7 for a plot as a function of the squeezing $|\zeta|$. The limit of this function for $|\zeta| \rightarrow \infty$ is $\frac{2}{5}$. This is above the limit for the simultaneous measurement.

-
- [1] W. Heisenberg, Über den anschaulichen Inhalt der quantentheoretischen Kinematik und Mechanik, *Z. Phys.* **43**, 172 (1927).
- [2] E. H. Kennard, Zur Quantenmechanik einfacher Bewegungstypen, *Z. Phys.* **44**, 326 (1927).
- [3] R. F. Werner and T. Farrelly, Uncertainty from Heisenberg to today, *Found. Phys.* **49**, 460 (2019).
- [4] E. P. Wigner, On the quantum correction for thermodynamic equilibrium, *Phys. Rev.* **40**, 749 (1932).
- [5] J. Neumann, *Mathematical Foundations of Quantum Mechanics* (Princeton University Press, Princeton, 2018).
- [6] L. Cohen, Generalized phase-space distribution functions, *J. Math. Phys.* **7**, 781 (1966).
- [7] E. P. Wigner, *Perspectives in Quantum Theory*, edited by W. Yourgrau and A. Merwe (MIT Press, Cambridge, 1971), Chap. 4, pp. 25–36.
- [8] E. Arthurs, Jr. and J. L. Kelly, On the simultaneous measurement of a pair of conjugate observables, *Bell Syst. Tech. J.* **44**, 725 (1965).
- [9] E. Arthurs and M. S. Goodman, Quantum Correlations: A Generalized Heisenberg Uncertainty Relation, *Phys. Rev. Lett.* **60**, 2447 (1988).
- [10] R. F. Werner, Uncertainty relations for general phase spaces, *Front. Phys.* **11**, 110305 (2016).
- [11] S. Hacohe-Gourgy, L. S. Martin, E. Flurin, V. V. Ramasesh, K. B. Whaley, and I. Siddiqi, Quantum dynamics of simultaneously measured non-commuting observables, *Nature (London)* **538**, 491 (2016).
- [12] A. Chantasri, J. Atalaya, S. Hacohe-Gourgy, L. S. Martin, I. Siddiqi, and A. N. Jordan, Simultaneous continuous measurement of noncommuting observables: Quantum state correlations, *Phys. Rev. A* **97**, 012118 (2018).
- [13] M. M. Weston, M. J. W. Hall, M. S. Palsson, H. M. Wiseman, and G. J. Pryde, Experimental Test of Universal Complementarity Relations, *Phys. Rev. Lett.* **110**, 220402 (2013).
- [14] G. Pütz, T. Barnea, N. Gisin, and A. Martin, Experimental weak measurement of two non-commuting observables, [arXiv:1610.04464](https://arxiv.org/abs/1610.04464).
- [15] A. C. Dada, W. McCutcheon, E. Andersson, J. Crickmore, I. Puthoor, B. D. Gerardot, A. McMillan, J. Rarity, and R. Oulton, Optimal simultaneous measurements of incompatible observables of a single photon, *Optica* **6**, 257 (2019).
- [16] N. G. Walker and J. E. Carroll, Multiport homodyne detection near the quantum noise limit, *Opt. Quantum Electron.* **18**, 355 (1986).
- [17] M. Freyberger, K. Vogel, and W. P. Schleich, From photon counts to quantum phase, *Phys. Lett. A* **176**, 41 (1993).
- [18] W. Vogel and D.-G. Welsch, *Quantum Optics* (Wiley-VCH, Weinheim, 2006).
- [19] C. Gerry and P. Knight, *Introductory Quantum Optics* (Cambridge University Press, Cambridge, 2004), p. 17.
- [20] K. Vogel and H. Risken, Determination of quasiprobability distributions in terms of probability distributions for the rotated quadrature phase, *Phys. Rev. A* **40**, 2847 (1989).
- [21] D. T. Smithey, M. Beck, M. G. Raymer, and A. Faridani, Measurement of the Wigner Distribution and the Density Matrix of a Light Mode Using Optical Homodyne Tomography: Application to Squeezed States and the Vacuum, *Phys. Rev. Lett.* **70**, 1244 (1993).
- [22] U. Leonhardt and H. Paul, High-Accuracy Optical Homodyne Detection with Low-Efficiency Detectors: “Preamplification” from Antisqueezing, *Phys. Rev. Lett.* **72**, 4086 (1994).
- [23] S. Wallentowitz and W. Vogel, Unbalanced homodyne for quantum state measurements, *Phys. Rev. A* **53**, 4528 (1996).
- [24] G. Breitenbach, S. Schiller, and J. Mlynek, Measurement of the quantum states of squeezed light, *Nature (London)* **387**, 471 (1997).
- [25] A. Luis, J. Sperling, and W. Vogel, Nonclassicality Phase-Space Functions: More Insight with Fewer Detectors, *Phys. Rev. Lett.* **114**, 103602 (2015).
- [26] M. Bohmann, J. Tiedau, T. Bartley, J. Sperling, C. Silberhorn, and W. Vogel, Incomplete Detection of Nonclassical Phase-Space Distributions, *Phys. Rev. Lett.* **120**, 063607 (2018).
- [27] J. Tiedau, V. S. Shchesnovich, D. Mogilevtsev, V. Ansari, G. Harder, T. J. Bartley, N. Korolkova, and C. Silberhorn, Quantum state and mode profile tomography by the overlap, *New J. Phys.* **20**, 033003 (2018).
- [28] E. Knyazev, K. Y. Spasibko, M. V. Chekhova, and F. Y. Khalili, Quantum tomography enhanced through parametric amplification, *New J. Phys.* **20**, 013005 (2018).
- [29] S. Olivares, A. Allevi, G. Caiazzo, M. G. A. Paris, and M. Bondani, Quantum tomography of light states by photon-number-resolving detectors, *New J. Phys.* **21**, 103045 (2019).
- [30] U. Leonhardt and H. Paul, Realistic optical homodyne measurements and quasiprobability distributions, *Phys. Rev. A* **48**, 4598 (1993).
- [31] A. Zucchetti, W. Vogel, and D.-G. Welsch, Quantum-state homodyne measurement with vacuum ports, *Phys. Rev. A* **54**, 856 (1996).
- [32] J. Řeháček, Y. S. Teo, Z. Hradil, and S. Wallentowitz, Surmounting intrinsic quantum-measurement uncertainties in Gaussian-state tomography with quadrature squeezing, *Sci. Rep.* **5**, 12289 (2015).
- [33] G. Gallot and D. Grischkowsky, Electro-optic detection of terahertz radiation, *J. Opt. Soc. Am. B* **16**, 1204 (1999).
- [34] C. Riek, D. V. Seletskiy, A. S. Moskalenko, J. F. Schmidt, P. Krauspe, S. Eckart, S. Eggert, G. Burkard, and A. Leitenstorfer,

- Direct sampling of electric-field vacuum fluctuations, *Science* **350**, 420 (2015).
- [35] A. S. Moskaleiko, C. Riek, D. V. Seletskiy, G. Burkard, and A. Leitenstorfer, Paraxial Theory of Direct Electro-Optic Sampling of the Quantum Vacuum, *Phys. Rev. Lett.* **115**, 263601 (2015).
- [36] C. Riek, P. Sulzer, M. Seeger, A. S. Moskaleiko, G. Burkard, D. V. Seletskiy, and A. Leitenstorfer, Subcycle quantum electrodynamics, *Nature (London)* **541**, 376 (2017).
- [37] M. Kizmann, T. L. M. Guedes, D. V. Seletskiy, A. S. Moskaleiko, A. Leitenstorfer, and G. Burkard, Subcycle squeezing of light from a time flow perspective, *Nat. Phys.* **15**, 960 (2019).
- [38] T. L. M. Guedes, M. Kizmann, D. V. Seletskiy, A. Leitenstorfer, G. Burkard, and A. S. Moskaleiko, Spectra of Ultrabroadband Squeezed Pulses and the Finite-Time Unruh-Davies Effect, *Phys. Rev. Lett.* **122**, 053604 (2019).
- [39] I.-C. Bena-Chelms, F. F. Settembrini, G. Scalari, and J. Faist, Electric field correlation measurements on the electromagnetic vacuum state, *Nature (London)* **568**, 202 (2019).
- [40] F. Lindel, R. Bennett, and S. Y. Buhmann, Theory of polaritonic quantum-vacuum detection, *Phys. Rev. A* **102**, 041701(R) (2020).
- [41] F. Lindel, R. Bennett, and S. Y. Buhmann, Macroscopic quantum electrodynamics approach to nonlinear optics and application to polaritonic quantum-vacuum detection, *Phys. Rev. A* **103**, 033705 (2021).
- [42] M. Kizmann, A. S. Moskaleiko, A. Leitenstorfer, G. Burkard, and S. Mukamel, Quantum susceptibilities in time-domain sampling of electric field fluctuations, *Laser Photon. Rev.* **16**, 2100423 (2022).
- [43] S. Onoe, T. L. M. Guedes, A. S. Moskaleiko, A. Leitenstorfer, G. Burkard, and T. C. Ralph, Realizing a rapidly switched Unruh-DeWitt detector through electro-optic sampling of the electromagnetic vacuum, *Phys. Rev. D* **105**, 056023 (2022).
- [44] S. Namba, Electro-optical effect of zincblende, *J. Opt. Soc. Am.* **51**, 76 (1961).
- [45] R. Boyd, *Nonlinear Optics* (Academic, London, 2020), Chap. 11.
- [46] O. Steuernagel and S. Scheel, Approaching the Heisenberg limit with two-mode squeezed states, *J. Opt. B* **6**, S66 (2004).
- [47] S. Steinlechner, J. Bauchrowitz, M. Meinders, H. Müller-Ebhardt, K. Danzmann, and R. Schnabel, Quantum-dense metrology, *Nat. Photon.* **7**, 626 (2013).
- [48] W. Du, J. F. Chen, Z. Y. Ou, and W. Zhang, Quantum dense metrology by an SU(2)-in-SU(1,1) nested interferometer, *Appl. Phys. Lett.* **117**, 024003 (2020).
- [49] M. Ast, S. Steinlechner, and R. Schnabel, Reduction of Classical Measurement Noise via Quantum-Dense Metrology, *Phys. Rev. Lett.* **117**, 180801 (2016).
- [50] L. Vaidman, Teleportation of quantum states, *Phys. Rev. A* **49**, 1473 (1994).
- [51] S. L. Braunstein and H. J. Kimble, Teleportation of Continuous Quantum Variables, *Phys. Rev. Lett.* **80**, 869 (1998).
- [52] C. Weedbrook, A. M. Lance, W. P. Bowen, T. Symul, T. C. Ralph, and P. K. Lam, Quantum Cryptography Without Switching, *Phys. Rev. Lett.* **93**, 170504 (2004).
- [53] A. M. Lance, T. Symul, V. Sharma, C. Weedbrook, T. C. Ralph, and P. K. Lam, No-Switching Quantum Key Distribution Using Broadband Modulated Coherent Light, *Phys. Rev. Lett.* **95**, 180503 (2005).
- [54] A. N. Jordan and M. Büttiker, Continuous Quantum Measurement with Independent Detector Cross Correlations, *Phys. Rev. Lett.* **95**, 220401 (2005).
- [55] P. Sulzer, K. Oguchi, J. Huster, M. Kizmann, T. L. M. Guedes, A. Liehl, C. Beckh, A. S. Moskaleiko, G. Burkard, D. V. Seletskiy, and A. Leitenstorfer, Determination of the electric field and its Hilbert transform in femtosecond electro-optic sampling, *Phys. Rev. A* **101**, 033821 (2020).
- [56] R. J. Glauber, Coherent and incoherent states of the radiation field, *Phys. Rev.* **131**, 2766 (1963).
- [57] E. C. G. Sudarshan, Equivalence of Semiclassical and Quantum Mechanical Descriptions of Statistical Light Beams, *Phys. Rev. Lett.* **10**, 277 (1963).
- [58] K. E. Cahill and R. J. Glauber, Density operators and quasiprobability distributions, *Phys. Rev.* **177**, 1882 (1969).
- [59] H. J. Carmichael, *Statistical Methods in Quantum Optics I* (Springer, Berlin, 1999), p. 110.
- [60] K. Husimi, Some formal properties of the density matrix, *Proc. Phys.-Math. Soc. Jpn. 3rd Ser.* **22**, 264 (1940).
- [61] T. L. M. Guedes, I. Vakulchyk, D. V. Seletskiy, A. Leitenstorfer, A. S. Moskaleiko, and G. Burkard, Back action in quantum electro-optic sampling of electromagnetic vacuum fluctuations, [arXiv:2202.03353](https://arxiv.org/abs/2202.03353).
- [62] H. P. Robertson, The uncertainty principle, *Phys. Rev.* **34**, 163 (1929).
- [63] C. Y. She and H. Heffner, Simultaneous measurement of non-commuting observables, *Phys. Rev.* **152**, 1103 (1966).
- [64] M. A. Ochoa, W. Belzig, and A. Nitzan, Simultaneous weak measurement of non-commuting observables: A generalized Arthurs-Kelly protocol, *Sci. Rep.* **8**, 15781 (2018).
- [65] T. Karmakar, P. Lewalle, and A. N. Jordan, Stochastic path-integral analysis of the continuously monitored quantum harmonic oscillator, *PRX Quantum* **3**, 010327 (2022).
- [66] W. H. Zurek, S. Habib, and J. P. Paz, Coherent States via Decoherence, *Phys. Rev. Lett.* **70**, 1187 (1993).
- [67] V. Bužek, R. Derka, G. Adam, and P. L. Knight, Reconstruction of quantum states of spin systems: From quantum Bayesian inference to quantum tomography, *Ann. Phys. (NY)* **266**, 454 (1998).
- [68] J. M. Bernardo and A. F. M. Smith, *Bayesian Theory* (Wiley-VCH, Weinheim, 1994).
- [69] M. A. Nielsen and I. L. Chuang, *Quantum Computation and Quantum Information* (Cambridge University Press, Cambridge, 2009), pp. 409–423.
- [70] S. L. Braunstein, C. M. Caves, and G. J. Milburn, Interpretation for a positive P representation, *Phys. Rev. A* **43**, 1153 (1991).
- [71] F. F. Settembrini, F. Lindel, A. M. Herter, S. Y. Buhmann, and J. Faist, Detection of quantum-vacuum field correlations outside the light cone, *Nat. Commun.* **13**, 3383 (2022).
- [72] J. G. Skellam, The frequency distribution of the difference between two Poisson variates belonging to different populations, *J. R. Stat. Soc.* **109**, 296 (1946).
- [73] D. Karlis and I. Ntzoufras, Bayesian analysis of the differences of count data, *Stat. Med.* **25**, 1885 (2006).